Journal of Climate

Changes in North American Atmospheric Circulation and Extreme Weather: Influence of Arctic Amplification and Northern Hemisphere Snow Cover

--Manuscript Draft--

Manuscript Number:	JCLI-D-16-0762
Full Title:	Changes in North American Atmospheric Circulation and Extreme Weather: Influence of Arctic Amplification and Northern Hemisphere Snow Cover
Article Type:	Article
Corresponding Author:	Stephen Jackson Vavrus, Ph.D. University of Wisconsin Madison, WI UNITED STATES
Corresponding Author's Institution:	University of Wisconsin
First Author:	Stephen Jackson Vavrus, Ph.D.
Order of Authors:	Stephen Jackson Vavrus, Ph.D.
	Fuyao Wang
	Jonathan Martin
	Jennifer Francis
	Yannick Peings
	Julien Cattiaux
Abstract:	This study tests the hypothesis that Arctic amplification (AA) of global warming remotely affects middle latitudes by promoting a weaker, wavier atmospheric circulation conducive to extreme weather. The investigation is based on the late-21st century over greater North America (20-90N, 50-160W) using 40 simulations from the Community Earth System Model's Large Ensemble, spanning 1920-2100. AA is found to promote regionally varying ridging aloft (500 hPa) with strong seasonal differences reflecting the location of strongest surface thermal forcing. During winter, maximum increases in future geopotential heights are centered over the Arctic Ocean, in conjunction with sea ice loss, but minimum height increases (troughing) occur to the south, over the continental United States. During summer the location of maximum height inflation shifts equatorward, forming an annular band across mid-high latitudes of the entire Northern Hemisphere. This band spans the continents, whose enhanced surface heating is aided by antecedent snow-cover loss and reduced terrestrial heat capacity. Through the thermal wind relationship, mid-tropospheric winds weaken on the equatorward flank of both seasonal ridging anomalies---mainly over Canada during winter and even more over the continental United States during summer---but strengthen elsewhere to form a dipole anomaly pattern in each season. Changes in circulation waviness, expressed as sinuosity, are inversely correlated with changes in zonal wind speed at nearly all latitudes, both in the projections and as observed during recent decades. Over the central United States during summer, the weaker and wavier flow promotes drying and enhanced heating, thus favoring more intense summer weather.

Powered by Editorial Manager® and ProduXion Manager® from Aries Systems Corporation

Click here to access/download
Cost Estimation and Agreement Worksheet
Cost Estimation and Agreement Worksheet.pdf

Response to Reviewers
Click here to download Response to Reviewers Response to Reviewers.docx

Dear Editor (John Walsh),

We have revised our manuscript based on the helpful feedback from you and the three reviewers. All of the critiques raise important questions and offer constructive suggestions for improvement, which we address in a point-by-point manner below.

Reviewer 1

1. Of course there is the issue that different models and different evaluation metrics of models gives different results. At least there are multiple ensembles used here. Perhaps the authors could say a bit more about what the range of ensemble results are.

The reviewer (and editor) notes that our study relies on a single GCM, although our approach has the advantage of containing multiple ensembles. We have illustrated the internal variability of this model (CESM) by showing the output of all the individual ensemble members overlain against the ensemble-mean in Figures 3 and 7. We also depict a measure of significance in Figures 6 and 7 by denoting where the ensemble-mean changes exceed the standard deviation of the intra-ensemble changes. To emphasize this point, we have added wording to lines 226-227 describing Figure 3 that the ensemble range of sinuosity is relatively small (in relation to the annual cycle). In addition, we added a statement at the end of the paragraph describing Figure 7 (lines 339-342) that the sign of the sinuosity changes is generally consistent among ensemble members at most latitudes and both seasons.

2. A real pay off of this paper is the existence of the dipole in figure 6c that has a difference between North America and Asia. This appears to be the link between Arctic and weather on the US side. This figure looks like the anomaly field rather than the height field as in the figure caption. Same for 6a anomalies???

All the panels in Figure 6 show the changes in mean climate between the late 21st century (average of 2081-2100) and the late 20th century (average of 1981-2000), as described in the caption.

3. I reviewed another paper that talked about the dipole structure that had more meridional southerlies over the central US based on data. Could this be a main result that adds North America to Asia for the existence of linkages argument? Perhaps make a bigger deal out of this as a prime conclusion. The paper said there is a trend for more heavy rainfall as the new meridional flow brought moisture up from the Gulf of Mexico. You talk of drying even on the event scale. Is this due to you looking at the end of 21st century when any heating overwhelms dynamic effects?

We aren't sure which paper the reviewer is referring to, so we can't address that paper's findings. However, moisture advection---or lack of it---from the Gulf of Mexico is known to be very important for triggering summertime rainfall over the Plains, so it makes sense that more heavy rainfall would be simulated in that study if more southerly flow occurred. The time frame of our two studies might well be critical, because the climate change signal becomes very large by the end of the 21st century, which is the interval of our focus. As illustrated in Figures 9 and 10, the projected circulation response favors a

reduction in Gulf inflow to the Plains during summer and thus causes a tendency for drier climatological conditions (Figure 8). Importantly, this regional drying pattern is commonly simulated by other climate models, as we noted in our Maloney et al. citation (line 360), and we buttress that finding in this revised manuscript by showing the similarity of LENS with the CMIP5 average model circulation change during summer (new Figure S4), which also consists of a ridging anomaly aloft that favors dry, warm subsiding air into the Plains. This resemblance suggests that our interpretation from CESM-CAM5 applies to models generally.

Reviewer 2

1. Most of the research on the effects of Arctic changes on mid-latitude weather and climate has so far focused on the effects of Arctic sea ice decline, in particular in autumn and winter. Now the authors demonstrate that major circulation changes are fostered by the enhanced summertime heating of continents in mid-high latitudes (e.g. lines 488-489). This is a very interesting result, which could be put more in front in the Abstract and perhaps even reflected in the title of the manuscript. Is "Arctic connection" the best wording in the title, if the effects originate from "mid-high latitudes"?

We agree with the reviewer that the enhanced summertime heating of continents is an interesting result and that it encompasses more than just the traditional Arctic domain. The abstract does describe this finding: "This [annular ridging band] spans the continents, whose enhanced surface heating is aided by antecedent snow-cover loss and reduced terrestrial heat capacity." Because the reduction of snow cover extends beyond a traditional definition of the Arctic (Figure 11), we have taken the reviewer's advice to reconsider the wording of our title. We modify it in this revised version to become "Changes in North American Atmospheric Circulation and Extreme Weather: Influence of Arctic Amplification and Northern Hemisphere Snow Cover".

Also, as the Arctic amplification is a central concept in the manuscript, it would be good to better explain how the "mid-high latitude" warming contributes to the Arctic amplification. It would also be relevant to refer to Crawford and Serreze (2015), who have so well demonstrated the summer warming of terrestrial Arctic/sub-Arctic.

The "mid-high latitude" warming contributes to Arctic amplification through terrestrial summertime heating that is enhanced by the factors described in the text: snow cover loss, prevalence of continents in higher latitudes (peak land cover fraction at 65^{o}N), and lower heat capacity of land compared with water. The importance of these factors operating precisely within a traditional Arctic domain (e. g., poleward of 60^{o}N) versus equatorward of that region is difficult to determine, and therefore some of the enhanced terrestrial warming during summer contributes to Arctic amplification in an indirect way (we have therefore modified the Section 3.4 subheading from "Role of high latitudes" to "Role of higher latitudes"). However, most of the annular ridging band attributable to snow cover loss in the idealized modeling experiment occurs north of 50^{o}N, consistent with the ridging

anomaly band in the late-21st century shown in Figure 6d, suggesting a significant contribution from snow cover. We thank the reviewer for pointing us to the Crawford and Serreze (2015) paper, which indeed nicely demonstrates the role of snow-cover loss in enhancing the heating of land during summer. We have added a citation to this study at line 418.

2. The authors could consider adding in the discussion section that climate-scale modelling of a regional atmospheric circulation response to thermodynamic forcing is, in general, liable to errors, and ideally should be based on more than one climate model (even if a good one is used in the present study). Also, considering results for regional changes in precipitation, so far climate models have captured the overall wetting trends in the Arctic but had problems in reproducing the regional patterns (Lique et al., 2016, JGR) (I am not sure if it is easier to model the future changes in the central U.S. than the past changes in the Arctic).

Good point about the usefulness of applying more than one climate model to identify robust conclusions. Fortunately, CESM-CAM5 simulates large-scale circulation changes under greenhouse forcing that are strikingly similar to the typical CMIP5 model in both winter and summer (see new Figure S4). As for the regional rainfall changes over the central U. S. in CESM-CAM5, these also resemble the summertime drying pattern over the U. S. Great Plains produced by the CMIP5 model average for RCP8.5 (Maloney et al. 2014).

3. Lines 242-247: it is not clear for me how the complication is circumvented.

We can avoid the complication by shifting the reference frame from individual geopotential height contours, which can migrate in a warming climate, to a fixed reference frame of individual latitudes. By expressing sinuosity as a function of latitude, the SIN metric quantifies how the waviness at a fixed location in space changes with time, regardless of whether the overlying isohypses are migrating.

4. Line 472. Is the causal relationship such that AO influences the waviness of the jet stream, or do we get a negative AO when the jet stream is wavy?

That's a great question that goes beyond the scope of this response. There is evidence that Rossby wave breaking can shape the phase of the AO (such as Woolings et al., 2008, JAS), but the point we're making is simply that the jet stream tends to be wavier when the AO is in its negative phase (e. g., Figure 4). To keep readers from inferring causality, we have modified Line 483 from saying that the interannual variations of waviness are "influenced by" the AO to saying that they are "associated with the phase of the AO".

5. Figure 8. It seems that the same colour scale cannot be valid for the upper and lower plots (compare numbers given on line 346).

Thank you for bringing this to our attention. We have modified Figure 8 accordingly.

6. The authors use the term "surface temperature" when they evidently mean the near-surface (2 m) air temperature. This is a common practice in climatology, but I would avoid it in

studies that address the effects of surface temperature anomalies (e.g. due to snow melt) on air temperature.

Good point. We have changed the text and figure captions accordingly.

Reviewer 3

1. Line 80: this sentence could be slightly misleading: Di Capua and Coumou (2016) did not analyze future projections; I would suggest rewriting the sentence so that the content of each of the three cited papers is correctly reported.

Agreed. We have rewritten the sentence to be clearer about the data used in each study.

2. Figure 1-middle panel: figure 1 nicely explains the adopted methodology, would it be possible to add the equivalent latitude also for the American sector as in the left panel? I think this could further help the reader to understand how the SIN index is defined.

This is a good suggestion, and we tried doing so in the revision. Unfortunately, the overlain equivalent latitude lines made the figure too busy and thus distracted from our already complicated explanation of sinuosity. Therefore, we decided to stick with the original version of Figure 1.

3. Figure 1-right panel: it seems that the right panel is described in the text but not in the figure caption, this can be confusing at first sight.

Figure 1 requires a lot of explanation of the sinuosity method. We originally tried explaining everything in the caption, but the caption became far too long (it's already lengthy). Therefore, we decided to cover in the text the less critical information shown in the right hand-hand panel. We direct the reader to the text for additional explanation at the end of the caption.

4, Figure 3-a: would it be possible to calculate the correlation between SIN and wind speed on daily basis over the whole time series? From the behavior of the annual cycle, I would expect a strong negative correlation, is this true?

Good idea. We calculated the daily correlation between ASIN and zonal wind speed in Figure 3a over the whole time series and obtained a strong r = -0.61 relationship (r = -0.93 based on climatology). We've added this information to the text in lines 216-218.

5. Figure 3-b: I am a little bit concerned that the same range of isohypses is analyzed for all four seasons; in particular for the warm season, the 5280 and 5400 m migrate really far north and I would not rely on those to describe the circulation of the mid-latitudes. Could the author(s) provide a sensitivity analysis on the influence of the chosen isohypses on the ASIN index? Or provide an analysis of the mean latitude at which these isohypses are found in each season?

The reviewer raises one of the challenges of the aggregate sinuosity (ASIN) method: what choice of isohypses best represents mid-latitude circulation throughout the year? We have tested various sets of isohypses and finally settled on the five described in the article. However, the reviewer is correct that the 5280 and 5400 m contours migrate quite far north during the summer. Fortunately, aggregate sinuosity is a weighted average based on all five of these isohypse lengths, such that the lowest weights are assigned to the shortest (most northerly) isohypses (see formula on line 165). As a result, these northerly contours have the smallest influence on ASIN in every season, and their impact during summer is particularly weak, because on some summer days they do not even occur over the domain (when the atmosphere is especially warm). To underscore this point, a comparison of the annual cycle of ASIN in Figure 3a with the annual cycle of sinuosity among each of the five isohypses in Figure 3b shows that the 5280 m and 5400 m height contours contribute the least to ASIN. Instead, the shape of the ASIN annual cycle is best explained as a combination of the 5640 m and 5520 m isohypses, which are in the middle of the five-isohypse set.

6. Line 180: I agree with the author(s) that expressing the SIN as function of the latitude can indeed help to avoid the problem of the northward shift of the isohypses, though while reading the paper I was a little bit confused on how this was accomplished: does it refer only to figure 5 and figure 7? Has a certain range of latitudes values been averaged to obtain the ASIN or did the author(s) try to select different latitudinal ranges? Or to define the ASIN also on latitudinal basis? I would suggest to stress more which methodologies have been used and where, in particular in line 165, does the formula refers to the SIN or to the ASIN?

Yes, the calculation of sinuosity as a function of latitude is only applied to Figures 5 and 7 (and Figure S5 of supplementary material). We realize now that we should have been clearer in distinguishing between SIN, which refers to sinuosity generally and as a function of latitude, and ASIN, which is strictly the aggregate sinuosity (i. e., the weighted average of the sinuosity of the five individual isohypses we targeted: 576 dm, 564 dm, 552, dm, 540 dm, and 528 dm). One critical oversight is that we failed to use "ASIN" in the formula defining aggregate sinuosity in line 165. That change alone should help readers a lot. In addition, we have gone through the text and altered the use of "SIN" and "ASIN" where appropriate to make this distinction more apparent.

7. Figure 5: interesting plot, I am surprised that the trends in the latest two decades are not significant; does it depend on the reduced length of the time series? How would the same plot look like if the trend is calculated on the whole time series? Would it be significant?

The absence of a significant trend in the past two decades is surprising, but the reason is indeed the shortness of the recent record (and the inherently high variability in the Arctic). Because Figure 5 shows moving linear trends, the question about significance for the entire length of the time series can be answered by looking at the very beginning year (1948). Only in a few places are the trends significant over the whole record.

8. Figure 7: would it be possible to calculate the correlation between the wind speed and the

ASIN, for each latitude? In the August panel it must be noted that around 45°N almost the same change in wind speed produces (if we assume that that is the cause) a very different response in the change of sinuosity if compared with 60°N or with the January panel, can this be explained somehow?

Because sinuosity is a zonally averaged quantity, we can't calculate a correlation between wind speed and sinuosity at each latitude. However, the reviewer's main point is very valid that the 2 m/s wind speed reduction at 60°N in January corresponds to only a small increase in sinuosity at that latitude, yet the same wind speed change around 40°N in August corresponds to a very large increase in sinuosity. We touched on the reason for this heightened summertime sensitivity in the original text, attributing it to more closed highs aloft in the future, but we have elaborated on this point in the revised version (lines 331-334), because it is an interesting feature.

9. Figure 12: I found the color bars of left panels a bit confusing, it seems to me that there are unused colors, which give the impression that changes in the left panels are much smaller in magnitude than those in the right panels, while the range of change looks kind of the same.

Good point. We have tweaked the color bars and scales in Figure 12 accordingly.

10. In general, it is hard to link zonal wind speed with sinuosity of isohypses in a causal sense only with a qualitative analysis. In figure 7, we can see a very different response of the sinuosity to the same amplitude of wind forcing, (Jan ~60°N almost no changes in SIN, and Aug ~45°N +0.8 in SIN). Even a strong negative correlation might not imply causality unless supported by other data (further model experiments?). Moreover, geostrophic winds directly stem from gph, sinuosity describes gph field characteristics, thus changes in gph might produce changes in both variables, even though the two variables are not directly influencing each other. Thus, I would suggest to cautiously discuss the wind speed-meandering relation and concentrate mainly on the results themselves, which are indeed very interesting.

We agree with the words of caution suggested by the reviewer and have revised the text accordingly. For example, we modified the first bullet of the Conclusions to say that observed waviness trends are *associated with* the phase of the AO, rather than "influenced by" the AO. In addition, we have softened the statement on line 527 that the weakened zonal wind on the equatorward flank of anomalous future ridging "in turn leads to a wavier (more sinuous) flow". This statement has been reworded to say that the anomalous future ridging "weakens the zonal wind on the equatorward flank and leads to a weaker (wavier) flow" (i. e., no attribution of the weaker wind causing a wavier flow).

<u>Editor</u>

1. Limitations of reliance on only one model (CESM-CAM5 in this case)

Yes, the results of a single model should raise caution flags. We have addressed this point in our responses to Reviewers 1 and 2 and underscore it with our new Figure S4, which shows the average circulation response of CMIP5 models during January and August.

The resemblance of CMIP5 to CESM-CAM5 is remarkable and suggests that our analysis using a single model is representative of other state-of-the-art GCMs.

2. "Cause and effect" issues are lurking in several comments

We have addressed these issues in our responses to the reviewers by rewording certain statements to avoid attribution without evidence.

3. My own reading left me confused about the difference between the two indices, SIN and ASIN (lines 160-171).

Sorry about the confusion. See our reply to point #6 of Reviewer 3.

Click here to access/download
Additional Material for Reviewer Reference
Text_revised_markup.pdf

Manuscript (non-LaTeX)
Click here to download Manuscript (non-LaTeX) Text_revised_clean.docx

Changes in North American Atmospheric Circulation and Extreme Weather: Influence of Arctic Amplification and Northern Hemisphere Snow Cover

[1]Stephen J. Vavrus, [1]Fuyao Wang, [2]Jonathan E. Martin, [3]Jennifer A. Francis, [4]Yannick Peings, and [5]Julien Cattiaux

Submitted to *Journal of Climate*

[1]Nelson Institute Center for Climatic Research, University of Wisconsin-Madison, Madison, WI

[2]Department of Atmospheric and Oceanic Sciences, University of Wisconsin-Madison, Madison, WI

[3]Department of Marine and Coastal Studies, Rutgers University, New Brunswick, NJ

[4]Department of Earth Systems Science, University of California-Irvine, Irvine, CA

[5]Centre National de Recherches Meteorologiques, UMR 3589 CNRS/Meteo-France, Toulouse, France

Corresponding author: Stephen Vavrus (sjvavrus@wisc.edu); 1225 W. Dayton Street; Madison, WI 53706

Abstract

This study tests the hypothesis that Arctic amplification (AA) of global warming remotely affects middle latitudes by promoting a weaker, wavier atmospheric circulation conducive to extreme weather. The investigation is based on the late-21st century over greater North America (20°-90°N, 50°-160°W) using 40 simulations from the Community Earth System Model's Large Ensemble, spanning 1920-2100. AA is found to promote regionally varying ridging aloft (500 hPa) with strong seasonal differences reflecting the location of strongest surface thermal forcing. During winter, maximum increases in future geopotential heights are centered over the Arctic Ocean, in conjunction with sea ice loss, but minimum height increases (troughing) occur to the south, over the continental United States. During summer the location of maximum height inflation shifts equatorward, forming an annular band across mid-high latitudes of the entire Northern Hemisphere. This band spans the continents, whose enhanced surface heating is aided by antecedent snow-cover loss and reduced terrestrial heat capacity. Through the thermal wind relationship, mid-tropospheric winds weaken on the equatorward flank of both seasonal ridging anomalies---mainly over Canada during winter and even more over the continental United States during summer---but strengthen elsewhere to form a dipole anomaly pattern in each season. Changes in circulation waviness, expressed as sinuosity, are inversely correlated with changes in zonal wind speed at nearly all latitudes, both in the projections and as observed during recent decades. Over the central United States during summer, the weaker and wavier flow promotes drying and enhanced heating, thus favoring more intense summer weather.

1. Introduction

Numerous studies have suggested a relationship between mid-latitude weather and Arctic amplification (AA) of global climate change (e. g., Newson 1973, Honda et al. 2009, Petoukhov and Semenov 2010, Liu et al. 2012, Cohen et al. 2014, Coumou et al. 2015). Francis and Vavrus (2012), hereafter FV12, and Overland et al. (2015) described a proposed chain of causality, linking AA to a reduced meridional geopotential height gradient aloft, which leads to weaker upper-air extratropical westerlies, a wavier circulation, and the promotion of more frequent and persistent circulation patterns that favor extreme weather. Empirical evidence demonstrates a strong relationship between extreme weather events and slow moving, high-amplitude wave patterns (Thompson and Wallace 2001, Meehl and Tebaldi 2004, Petoukhov et al. 2013, Screen and Simmonds 2014), but whether AA actually forces such remote circulation changes remains in question (Vihma 2014, Walsh 2014, Cohen et al. 2014). Moreover, this hypothesized correlation is complicated by recent studies showing that expressions of Arctic-midlatitude teleconnections are probably regionally dependent (Overland et al. 2015, Kug et al. 2015). Furthermore, while the connection between a reduced meridional pressure gradient and a weaker zonal wind stems directly from thermal wind considerations, the subsequent linkage between a weaker zonal wind promoting enhanced meridional flow is harder to establish. In part this difficulty arises because different metrics have been used to quantify waviness, which has led to varying conclusions about recent trends in blocking and other high-amplitude patterns (Screen and Simmonds 2013, Barnes et al. 2014, Kennedy et al. 2016, Francis and Vavrus 2015, hereafter FV15).

71 The purpose of this study is to test the FV12 hypothesis under very strong greenhouse
72 forcing, over a single geographic domain, and using multiple model realizations to improve
73 the signal-to-noise ratio, which is relatively weak in observational studies that span only
74 the recent short period of enhanced Arctic warming (since mid/late-1990s). We focus on
75 the projected late-21st century climate change over greater North America (20°-90°N, 50°-
76 160°W) using 40 realizations from the Community Earth System Model's Large Ensemble
77 (LENS) (Kay et al. 2015). For comparison, we also analyze observed trends using the
78 NCEP-NCAR Reanalysis I (NNR, Kalnay et al., 1996) from 1948 to 2014. A similar
79 methodology has recently been applied to analyze the strength and waviness of the mid-
80 latitude circulation on a hemispheric scale using LENS (Peings et al. 2016), reanalyses (Di
81 Capua and Coumou 2016), and a combination of data from reanalyses and the Coupled
82 Model Intercomparison Version 5 (CMIP5) (Cattiaux et al. 2016). All of these studies
83 identified changes in mid-latitude circulation that varied seasonally and regionally, but
84 their focus was not exclusively North America. In addition, their reference location for
85 representing the extratropics was fixed at a single latitude, which is a useful approach for
86 succinctly characterizing aggregate circulation but potentially limiting in capturing
87 variations within geographic sectors. A similar regionally-averaged perspective using
88 CMIP5 output was provided by Barnes and Polvani (2015), who described projected mid-
89 latitude circulation changes over the North America-Atlantic region based on the average
90 response from 30°-70°N.

91 In this study, we extend these prior findings by revealing a more complete spatial
92 picture of greenhouse-forced climate changes within the North American region. As in
93 prior studies, our analysis considers changes in both the speed and waviness of the

94 atmospheric circulation and their implications for extreme weather. Following Cattiaux et
95 al. (2016) and Peings et al. (2016), we quantify waviness using the metric of sinuosity (SIN),
96 a common metric in geomorphology to measure the waviness of streams that was
97 described by Martin et al. (2016) as a way to characterize mid-tropospheric atmospheric
98 circulation. Di Capua and Coumou (2016) employed a similar metric called the meandering
99 index (M). Strongly zonal flow patterns result in low values of SIN and M, whereas very
100 meridional patterns yield high SIN and M. Based on the FV12 hypothesis, we expect that
101 Arctic amplification will contribute to a weaker and more sinuous circulation in middle
102 latitudes.

103 Here we extend these related recent studies by presenting SIN as a function of latitude
104 to identify potentially distinct responses in the behavior of the circulation across the vast
105 expanse of the extratropics (20^{o}-90^{o}N) over greater North America. Rather than
106 considering the entire Northern Hemisphere, we adopt a regional focus for several reasons.
107 First, shrinking the domain reduces the risk of diluting the signal when combining sectors
108 whose flow becomes more zonal with sectors trending toward more meridional circulation.
109 Second, extreme weather has been increasing in recent years over this region, based on the
110 United States Climate Extremes Index (Gleason, 2008), featuring many high-profile events
111 such as Superstorm Sandy in 2012 and the so-called "polar vortex" in 2014. Third, this
112 region experiences the clearest dipole pattern of projected future changes in zonal winds
113 aloft and thus serves as a useful testbed for the expected relationship between waviness
114 and circulation strength. Fourth, the North American domain encompasses a distinct
115 climatological ridge-trough couplet from west to east (Singh et al, 2016), providing a
116 clearly defined wave structure for computing sinuosity. Fifth, recent research has found a

117 strong regional dependence on the teleconnections between Arctic change and mid-
118 latitude weather (e.g., Overland et al., 2015 and references therein).

119

120 **2. Data and methods**

121 We utilize 500 hPa daily geopotential heights and zonal wind speeds from both
122 atmospheric reanalysis and global climate model simulations. The reanalysis data are from
123 the NCEP-NCAR Reanalysis I (NNR, Kalnay et al., 1996), with horizontal resolution of 2.5°
124 by 2.5° degree and spanning 1948 to 2014. Similar results are obtained using data from
125 European Center for Medium-Range Weather Forecasts (ECMWF) Reanalysis data (ERA-
126 40) and ERA-Interim, so only the findings from NNR are shown here. The simulated
127 atmospheric data from both historical and projected (Representative Concentration
128 Pathways 8.5, RCP8.5) LENS simulations are from the Community Earth System Model
129 version 5 (CESM-CAM5), which produces one of the most realistic climatologies in the
130 Coupled Model Intercomparison Project Phase 5 (CMIP5) suite of models (Knutti et al.
131 2013). Furthermore, the projected changes in upper-air circulation in LENS closely
132 resemble the average CMIP5 pattern, suggesting that the findings identified here are
133 representative. Each of the 40 ensemble members within LENS uses historical radiative
134 forcing from 1920-2005 and RCP8.5 radiative forcing thereafter until 2100. Each model
135 realization differs from one another by only small round-off level variations in their
136 atmospheric initial conditions. The CESM-CAM5 version used here is the 1-degree
137 latitude/longitude configuration (0.9x1.25_gx1v6). The large size of the ensemble helps to
138 distinguish signals of change from internal noise.

The strength of the circulation is defined as the speed of the zonal wind aloft, taken at a standard mid-tropospheric reference level of 500 hPa, while the more challenging description of circulation waviness is achieved through the sinuosity (SIN) metric. As described in Cattiaux et al. (2016), SIN is defined as the ratio of the curvilinear length of a 500 hPa geopotential height contour (isophypse) to the perimeter of its equivalent latitude, where the contour and the equivalent latitude enclose the same area within the regional boundaries (Figure 1). Relating its usage here to the more common application of sinuosity in geomorphology, the length of an isophypse is analogous to the length of a stream, while the perimeter of its equivalent latitude is akin to the shortest distance between the starting and ending points of that stream. SIN thus quantifies atmospheric waviness by representing the departure of 500 hPa height contours (isohypses) from a purely zonal orientation, and it accounts for closed circulation systems such as blocking highs and cut-off lows.

As noted in Martin et al. (2016), other metrics have also been used to characterize the waviness of the large-scale circulation, such as the zonal index (Rossby and collaborators 1939), the circularity ratio (Rohli et al. 2005), high-amplitude wave frequency (FV15), effective diffusivity (Nakamura 1996), meandering index (Di Capua and Coumou 2016), and various versions of wave activity (Nakamura and Solomon 2010; Huang and Nakamura 2016; Chen et al. 2015). Although each of these measures provides particular insights into the waviness of the flow, sinuosity applied to large-scale geopotential height fields offers an attractively intuitive description of the circulation compared with related metrics.

To create a single value of SIN that characterizes waviness in middle latitudes, we follow Martin et al. (2016) by computing an aggregate sinuosity (ASIN) as a weighted

average by using a set of five 500 hPa isohypses (576 dm, 564 dm, 552 dm, 540 dm, and 528 dm) representative of the mid-latitude circulation:

$$ASIN = \frac{[L_{576} + L_{564} + L_{552} + L_{540} + L_{528}]}{[EL_{576} + EL_{564} + EL_{552} + EL_{540} + EL_{528}]},$$

where L represents the length and EL the equivalent length of the isohypse within the greater North American domain. By boiling down the entire regional circulation into a single index, the purpose of aggregate sinuosity is similar to that of Cattiaux et al. (2016) and Peings et al. (2016), who represented the whole mid-latitude circulation from 30°-70°N by calculating SIN at the approximate midpoint (~50°N). Likewise, Di Capua and Coumou (2016) applied their meandering index to the latitude of maximum daily waviness, around 60°N, but their index does not account for closed circulation features.

To obtain more information on the spatial variations of waviness within the domain, we also apply a more comprehensive method by expressing SIN as a function of latitude, rather than particular geopotential heights. We first calculate daily SIN for individual geopotential height contours from 4600 m to 6050 m in 10 m increments to obtain a quasi-continuous magnitude of sinuosity across a span of geopotential heights characteristic of the extratropics. This geopotential height range covers all values in both the historical and future climates. The second step is to compute the zonally averaged geopotential height across each latitude band on every day, as illustrated in the right panel of Figure 1. We then assign to each latitude the SIN corresponding to the height contour representing that

183 latitude. For example, the zonally averaged height at 30°N is 5730 m (red dot in Figure 1)
184 and thus 30°N is assigned the sinuosity of the 5730 m isohypse. If a zonally averaged
185 height occurs at more than one latitude, then the SIN at each of these latitudes is identical,
186 as shown for the 5430 m isohypse, whose sinuosity is assigned to 45°N, 67°N, and 73°N
187 (blue dots). Expressing SIN as a function of latitude accounts for the confounding effect of
188 inflating geopotential heights in a warming climate (Barnes 2013) and identifies potentially
189 different sub-regional changes in the magnitude of SIN, such as those hypothesized to occur
190 between places experiencing zonal wind increases versus decreases in the future.

191

192 **3. Results**

193 *3.1 Recent Past*

194 To illustrate how sinuosity can quantify exceptional circulation states, we show the
195 lowest and highest values of daily ASIN during the study period (Figure 2a,b). A very
196 zonally oriented flow with aggregate sinuosity of 1.04 occurred on 24 December 1951,
197 associated with an extremely positive Arctic Oscillation (AO) index of +3.47. In contrast,
198 the remarkably muddled circulation pattern of 13 May 1993 yielded a record high ASIN of
199 2.64, coincident with an extremely negative -2.92 AO index. Many extreme weather events
200 coincide with high values of ASIN, such as the extreme cold-air outbreak in the United
201 States in January 2014 and Superstorm Sandy in October 2012 (Figure 2c,d), both of which
202 occurred amid highly negative AO phases that are conducive to meridionally oriented
203 circulation patterns and anomalously weak zonal flow across much of the middle latitudes
204 (Thompson and Wallace, 2001).

205 The mean annual cycle of ASIN in reanalysis exhibits a pronounced seasonal migration,
206 ranging from a broad wintertime minimum around 1.3 to a somewhat narrower peak just
207 above 1.6 during late spring and early summer (Figure 3a). This cycle over the greater
208 North American domain is similar to the hemispheric average obtained in Martin et al.
209 (2016), while the alternative sinuosity definition used in Cattiaux et al. (2016) results in a
210 somewhat earlier annual maximum during spring. The higher waviness during warmer
211 months is consistent with the observed maxima in blocking frequency during springtime
212 (Barriopedro et al. 2006), cut-off lows during summer (Price and Vaughan 1992;
213 Kentarchos and Davies 1998), and atmospheric wavenumber in summer (Willson, 1975).
214 Throughout the year there is a strongly inverse relationship between ASIN and zonal wind
215 speed, such that waviness is higher (lower) when westerlies aloft are weaker (stronger),
216 conforming with empirical evidence (Walsh 2014) and theory (Chen et al. 2015, Wang and
217 Nakamura 2015, Huang and Nakamura 2016). The correlation coefficient between
218 aggregate sinuosity and zonal wind speed is -0.61 for all days in the time series and -0.93
219 based on the climatological annual cycle shown in Figure 3a.

220 The annual cycle of aggregate sinuosity can be explained by the seasonality of the
221 individual isohypses that constitute ASIN (Figure 3b). The more southerly isohypses (552,
222 564, and 576 dm) exhibit a peak during summer, indicating their dominant role in shaping
223 ASIN. By contrast, the remaining isohypses (528, 540 dm) feature a double peak, one in
224 spring and one in fall, which coincides with the prevalence of cut-off lows in more
225 northerly locations across the domain (Martin et al. 2016). During summer, these
226 isohypses migrate so far poleward that their meridional wave amplitude is constrained.
227 LENS reproduces these major circulation features in the ensemble mean and shows a

relatively small ensemble range (Figures 3c,d), closely simulating the phasing of the annual cycle but with a somewhat sharper and elevated summer maximum. Likewise, the model reproduces the major features of individual isohypses, although it simulates a more distinct summertime sinuosity peak of the southernmost contour (576 dm).

Annually averaged ASIN exhibits an upward trend over the course of the study period that is significant at the 99% level, based on the Sen-Kendall method (Sen 1968) and a Mann-Kendall test (Mann 1945). Imbedded within this positive tendency is pronounced interannual variability (Figure 4) related closely to the annual AO index ($r = -0.51$, 99% significance level). This relationship is apparent in the two highest ASIN years (2009 and 2010) that coincide with very negative AO indices during winter 2009-2010 (Cohen et al., 2010), as well as the lowest annual ASIN in more than 40 years (1990) occurring during the most positive AO year. Daily variations in ASIN are significantly associated with the AO throughout the year, ranging from correlations of -0.40 (November) to -0.53 (March), in agreement with Martin et al. (2016), Cattiaux et al. (2016), and Di Capua and Coumou (2016). The strongly inverse relationship between ASIN and the AO on daily to annual time scales indicates that sinuosity represents variations of circulation waviness prevailing across the middle latitudes as the polar vortex weakens and strengthens.

A potential problem with interpreting the long-term behavior of ASIN is that a warming climate inflates geopotential height contours, thus causing the reference isohypses to shift poleward and possibly confounding comparisons over time, as demonstrated by Barnes (2013). To circumvent this complication, we also examined trends in sinuosity by latitude during winter and summer (Figure 5), whose intra-seasonal trends are much more consistent than those in spring and autumn (not shown). The long-term behavior of SIN, as

expressed by moving linear trends, varies with time and season, but a noteworthy feature is the consistently positive trends during winter and summer beginning around 1980 in middle-high latitudes that largely account for the increasing annual ASIN. Interestingly, this timing coincides with the start of reliable satellite records of Arctic sea ice and certain reanalysis products, such as ERA-Interim (Dee et al. 2011), that have been used to diagnose recent Arctic climate change. These recent upward trends in SIN generally align with downward trends in zonal wind speed aloft (Figure 5), particularly during winter, reflecting their inverse relationship over the annual cycle shown in Figure 3 and interannually (Cattiaux et al., 2016; Peings et al. 2016).

3.2 Simulated Future Changes

Driven by strong greenhouse forcing, the simulated extratropical climate warms significantly in the future and features major circulation changes by late century. As shown in Figure 6, the 40-member LENS average produces two general patterns of 500 hPa geopotential height anomalies: one that occurs during winter (November to March), exemplified by January, and the other during summer (June to September), represented by August (individual months are presented in Figures S1-S3). The winter pattern is characterized by exceptionally strong surface heating in the Arctic, particularly over the Arctic Ocean (Figure 6a), which experiences dramatic reductions in sea ice extent and thickness (not shown). Remarkably, near-surface temperatures rise by up to 25 K in January and promote major positive mid-tropospheric height anomalies aloft over most of the Arctic, as well as across most of Eurasian middle latitudes. By contrast, heights fall in a relative sense to the south of the Arctic-based ridging anomaly, extending from the North

Pacific to northern Europe and bearing some resemblance to the negative phase of the Arctic Oscillation (Figure 6c). The associated changes in zonal winds are dictated by these pressure redistributions through the thermal wind relationship, such that weaker westerlies aloft across North America (centered mainly over Canada) are sandwiched between the anomalous ridging over the Arctic and anomalous troughing to the south, with maximum wind increases impinging on the southern California coast (Figure 6e). Conversely, the pressure redistribution over the eastern hemisphere causes a very different zonal wind response, featuring stronger speeds over most of western Europe but a widespread band of weaker westerlies across the entire southernmost part of the extratropics from the prime meridian to the date line.

The summertime climate changes (right side of Fig. 6) are very different from those during winter. There is a more uniform warming pattern over mid-high latitudes, with some of the most pronounced temperature increases occurring farther south, over mid-latitude continents (Figure 6b). Warming over western North America is particularly strong, reminiscent of recent years. This widespread surface warming is associated with very large geopotential height increases across the entire extratropics (Figure 6d), indicative of the overall warmer Northern Hemisphere during boreal summer. A more important seasonal difference is the configuration of maximum height increases, which in summer are oriented in an annular pattern approximately centered around the location of greatest ridging over the central Arctic during winter. This summertime shift causes fairly coherent spatial changes in the speed of the zonal winds, which weaken over the entire Northern Hemisphere around 40^{o}N and strengthen over most of the hemisphere around 60^{o}N (Figure 6f). The weakening of the westerlies is especially pronounced over North

297 America, reaching 3-4 m s^{-1} over the central United States, attributable to the enhanced
298 ridging anomaly over western Canada that extends across the continent (Figure 6d). This
299 synoptic pattern is highly conducive to extreme heat and drought over the central United
300 States (Chang and Wallace 1987, Mo et al., 1997, Rowell 2009) and is consistent with the
301 documented weakening of mid-latitude storm tracks and zonal wind in CMIP5 models
302 (Chang et al. 2012, Lehmann et al. 2014, Coumou et al. 2015, Brewer and Mass 2016). In
303 fact, the circulation changes in LENS during both winter and summer stem from
304 geopotential height responses that are strikingly similar to those in CMIP5 (Figure S4).

305 Despite the very different circulation responses between summer and winter, one
306 commonality is the dipole pattern of zonal wind changes that emerges in both seasons,
307 indicative of meridional shifts in the mean jet stream. This response is more complex than
308 a general weakening of the extratropical circulation induced by AA, as hypothesized by
309 FV12, but it closely conforms to the proposed mechanisms via the loss of sea ice and snow
310 cover. Consistent with expectations, the simulated AA in these experiments promotes
311 marine-based ridging over high latitudes during winter and terrestrial-based ridging over
312 the northern extratropics during summer, both of which cause weaker westerlies aloft on
313 their equatorward flanks. FV12 further hypothesized that the weaker circulation would
314 lead to a wavier flow, a prediction that can be tested using the sinuosity metric. Peings et al.
315 (2016) reported that late-21st century sinuosity in LENS decreased during winter and
316 increased during summer (JJA) across the Northern Hemisphere overall, but opposite
317 seasonal changes occurred in the North American sector. Because of the distinctly dipole
318 response of the simulated zonal wind changes over North America, we opt here for an
319 alternative to either using sinuosity or calculating sinuosity at a fixed latitude, as in Peings

et al. (2016). Instead, we calculate SIN at each latitude band to capture the potentially variable response of circulation waviness across greater North America.

The response of SIN and zonal wind is found to be highly inversely correlated, both in winter and summer (Figure 7, Figure S5). The ensemble-mean sinuosity during winter is consistently lower south of 40°N, where the zonal wind strengthens by up to 2 m s^{-1}. Poleward of 40°N the zonal wind slackens by up to 2 m s^{-1}, while SIN increases at almost all latitudes by approximately the same amount (0.05-0.10) and by nearly the same magnitude as the maximum decrease south of 40°N. Inversely related changes in zonal wind and SIN also occur during summer and feature higher SIN between 35°-50°N, in concert with weakened westerlies of up to 2 m s^{-1}. A striking feature is the pronounced peak increase in sinuosity of around 0.8 at 42°N that is consistent with the sharp jump in climatological summertime SIN between 50°N and 40°N in the 20th century (Figure S6), characterized by more closed highs aloft when the circulation weakens during late summer. Sinuosity is sensitive to the presence of closed cyclones and anticyclones, whose isohypse length is extensive relative to equivalent length, and thus these features are exceptionally wavy by our metric (Martin et al. 2016). In high latitudes the westerlies strengthen during August by up to 1.5 m s^{-1} at 60°N, collocated with a maximum SIN reduction of nearly 0.2, but then exhibit no significant changes poleward of 70°N, where SIN declines modestly. In both seasons, the changes in SIN south of 30°N are less reliable, due to difficulties in calculating this circulation metric where the wave structure becomes less coherent outside of the climatological westerlies. This increased uncertainty is illustrated by the large scatter among ensemble members in SIN changes at low latitudes during January, whereas the sign

342 of the sinuosity changes is generally consistent among ensemble members at other
343 latitudes in both seasons.

344

345 *3.3 Relationship with extreme weather*

346 Our findings from LENS demonstrate that significant but spatially variable changes in
347 the strength and waviness of the circulation over North America can be expected in the
348 future. Because a sluggish, sinuous flow is often associated with extreme weather (Screen
349 and Simmonds 2014, FV12), our results suggest that conditions will become more
350 favorable for such anomalies over Canada and Alaska during winter and over much of the
351 continental U. S. during summer. In particular, the very large sinuosity increase and
352 weaker winds centered over the middle of the U. S. during summer warrants closer
353 examination. The circulation change in this season should promote excess heat and
354 drought, consistent with evidence of reduced cyclone activity (Lehmann et al. 2014,
355 Coumou et al. 2015). Indeed, LENS simulates that interior North America will receive up to
356 1-2 mm day^{-1} less August rainfall (30-50%) in the future (Figure 8), roughly co-located
357 with enhanced surface warming evident in Figure 6b. The combination of these two
358 changes promotes a strong loss of soil moisture that favors extreme heat and severe aridity
359 in this region (Teng et al. 2016, Douville et al. 2016). Many climate model simulations have
360 produced accentuated summer rainfall reductions in the Great Plains, including CMIP5
361 (Maloney et al. 2014), although there is not a consensus on the cause(s).

362 Our results suggest that the mean change in the large-scale circulation promotes
363 enhanced heating and rainfall reductions, but the mean does not reveal the synoptic-scale

364 expression of this climate change in terms of daily weather. To gain insight on that
365 question, we first show the relationship in LENS between the strength of the flow aloft and
366 the associated daily near-surface temperature and rainfall during August, averaged over
367 the box of maximum drying in Figure 8 (35^{o}N-45^{o}N, 105^{o}W-100^{o}W) that also encompasses
368 the core of maximum zonal wind speed reduction. Simulated daily anomalies are a strong
369 function of zonal wind speed, such that days with the weakest westerlies (or even
370 easterlies) aloft are the warmest and driest (Figure 9a-d). This relationship becomes
371 especially strong and virtually monotonic in the future and features a particularly large
372 drop-off in rainfall at the far left tail of the distribution that represents light easterly winds
373 aloft. These results are consistent with prior studies that demonstrated a highly inverse
374 relationship between summer temperature and rainfall over the Midwest (Madden and
375 Williams 1978, Chang and Wallace 1987, Trenberth and Shea 2005).

376 This linkage between large-scale circulation and extreme weather means that the
377 overall weakening and amplification of the summertime flow aloft over interior North
378 America favors hotter and drier weather, but the breakdown of projected changes in the
379 distribution of wind speeds yields additional information (Figure 9e, f). The average
380 weakening of the zonal circulation aloft is expressed as fewer days with strong flow and
381 more days with weak flow. This change is especially pronounced for days with easterly
382 winds, which occur less than 2% of the time in the late 20th century but approximately 15%
383 in the future simulation. A cleaner comparison between the two time periods can be made
384 by calculating the percentage change in the frequency of wind speeds across the
385 distribution, using equal-sized bins that each occupy 5% of the total (Figure 9f). The shift
386 in the distribution produces highly asymmetric changes, such that the frequency of days

with easterlies or lightest westerlies increases much more (up to 375%) than the decline of strongest westerlies. Because days with light winds are coincident with the driest and warmest conditions during both time periods (Figures 9a-d), their spike in the future implies that circulation changes will contribute strongly to increased extreme summertime weather in this region.

Further insight into the relationship between large-scale circulation and weather impacts is found by compositing the large-scale circulation anomalies on the driest August months within the same box described above (Figure 10). During these extremely dry months, the simulated circulation consists of an anomalous ridge to the north of the maximum mid-continental drying with anomalous easterly flow. The strength of the ridge also builds in the future and reaches up to a 30 m anomaly, compared with 20 m in the late 20th century. These characteristic drought circulation patterns in both time periods resemble the mean summertime circulation change (Figure 6d) and the observed pattern during Midwestern droughts and heat waves (Mo et al. 1997, Lau and Nath 2012). This agreement provides further evidence that the mean shift toward a weaker, wavier summertime circulation favors drier, warmer conditions that promotes extreme aridity over the central U. S. This dynamical signature further suggests that the excessive future drying and heating in this region is unlikely to be caused exclusively by local soil-moisture feedbacks, but rather that this aridity signal is significantly influenced by large-scale circulation changes.

3.4 Role of higher latitudes

409 A central open question is whether the projected summertime mid-latitude circulation
410 changes are a direct consequence of AA. Although the traditional perspective is that the
411 dynamical contribution to mid-continental drying stems from a poleward expansion of the
412 Hadley circulation and eddy-driven jet (Lu et al. 2007, Rivière 2011) and thus is somewhat
413 independent of high-latitude changes, an alternative explanation is that AA also plays a
414 significant role by promoting the annular band of maximum ridging (Figure 6d) through
415 enhanced heating of mid-high latitude continents.

416 Several lines of reasoning support this interpretation of an Arctic influence. First,
417 simulated greenhouse warming causes a large reduction in continental snow cover during
418 spring and early summer (Figure 11), which promotes warming by lowering surface albedo
419 and soil moisture (Matsumura and Yamazaki 2012, Crawford and Serreze 2015). Second,
420 this enhanced surface warming is most pronounced in mid-high latitudes, where
421 hemispheric land cover is most prevalent (between 45^{o}-70^{o}N, peaking around 65^{o}N). Third,
422 the much lower heat capacity of land versus water causes continents to warm more than
423 adjacent oceans during summer, as is apparent in LENS (Figure 6b). Alexander et al.
424 (2010) showed that imposed snow cover reductions in the CAM3 AGCM caused mid-high
425 latitude ridging during spring and summer, while observations demonstrate a similar
426 relationship from interannual snow cover anomalies (Matsumura and Yamazaki 2012). In
427 addition, an experiment using the CCSM3 GCM with all terrestrial snow cover eliminated
428 (Vavrus 2007) produced amplified summertime surface warming locally and an annular
429 band of ridging aloft that resembles the pattern produced in LENS (Figure 12 left, Figure
430 S7). Furthermore, these terrestrially based heating sources can generate standing Rossby
431 waves that are advected downstream by adiabatic warming from descending air masses

and the prevailing westerlies aloft (Rowell 2009, Matsumura and Yamazaki 2012, Matsumura et al. 2014). Indeed, the strongest 500 hPa zonal winds during summer in the late-21st century LENS simulations (Figure S8) are closely aligned with the band of maximum 500 hPa height increases (Figure 6d), particularly over the oceans. In this manner, enhanced terrestrial warming during summer over mid-high latitudes can initiate the annular band of maximum ridging simulated by LENS, very similar to the circum-hemispheric band of 500 hPa height anomalies found to be most highly correlated with projected summer rainfall reductions over western North America and Europe from greenhouse forcing (Rowell 2009). Over North America, the location of the band of inflated heights that peaks over western Canada (Figure 6d) is highly conducive to the simulated rainfall reductions in the Plains.

An Arctic-oriented remote influence may exacerbate known factors related to local soil-moisture feedbacks (Wetherald and Manabe 1999, Gregory et al. 1997, Su et al. 2014) and an expanded sub-tropical aridity belt (Lu et al. 2007; Scheff and Frierson 2012) as sources of mid-continental drying during summer, and it could be an important contributor to promoting the ridging pattern favorable for drought that is also simulated in the CMIP5 ensemble (Figure S4, Maloney et al. 2014, Brewer and Mass 2016). Evidence from other studies also allows for non-traditional sources of possible teleconnective drivers, as in Rowell (2009) and Rowell and Jones (2006), who determined that remote circulation anomalies originating in the tropics contribute little to projected continental drying in Europe and North America. Similarly, Lu et al. (2007) concluded that future Hadley cell expansion and the associated poleward shift of the subtropical dry zone is unlikely to originate from tropical processes, but rather is highly correlated with the extratropical

455 tropopause height. The annular pattern of ridging anomalies identified here is different
456 from the circumglobal teleconnection (CGT) (Yang et al. 2009), because the ridging band in
457 LENS is much farther north and there is no characteristic ridge to the northwest of India in
458 LENS (a key feature of the monsoon-driven CGT). Also, the CGT structure is equivalent
459 barotropic, but the LENS response over land is a mix of barotropic and baroclinic (not
460 shown).

461 Further support for a terrestrially driven, high-latitude circulation contribution comes
462 from a CCSM4 paleoclimate simulation of 6,000 years ago, when differences in Earth's
463 orbital configuration caused much more summertime insolation in the Northern
464 Hemisphere, especially in high latitudes (Otto-Bliesner et al. 2006). As with greenhouse
465 forcing, the strongest summer warming occurred on mid-high latitude land and was also
466 associated with a circum-hemispheric band of 500 hPa height increases that resembles the
467 LENS response, despite widespread tropical *cooling* (Figure 12 right). Moreover, the
468 teleconnection identified by Meehl and Tebaldi (2004) of enhanced Indian monsoon
469 rainfall driving a mid-high latitude band of ridging under greenhouse forcing does not
470 explain the hemispheric-scale response in LENS. Although LENS also simulates greater
471 monsoonal rainfall in the future, summers with more (less) rainfall are instead associated
472 with lower (higher) geopotential heights aloft in a band stretching from Asia to North
473 America (Figure S9). By contrast, the strength of the zonal wind over the North American
474 sector was found by Peings et al. (2016) to have a strong negative correlation with the
475 magnitude of AA among LENS ensemble members. Deciphering the definitive role of
476 higher latitudes in the summertime circulation changes described here requires additional
477 investigation and will benefit from further modeling experiments.

4. Discussion and Conclusions

Our study leads to the following conclusions regarding atmospheric circulation changes over North America and their possible connection with the Arctic:

• We find evidence for an increasing trend in mean-annual waviness during the past several decades, superimposed on strong interannual variations associated with the phase of the AO, in agreement with Francis and Skific (2015), FV2015, and Di Capua and Coumou (2016).

• There is a strong inverse relationship between projected changes in zonal wind speed and waviness, consistent with the inter-model CMIP5 and intra-ensemble LENS correlations identified in Cattiaux et al. (2016) and Peings et al. (2016).

• This negative correlation occurs in both winter and summer, but the alignment of the circulation changes across the domain nearly reverses between seasons. A dipole pattern of weaker (stronger) westerlies arises in low-mid latitudes during summer (winter), and generally stronger (weaker) westerlies develop in higher latitudes during summer (winter).

• Simulations suggest a trend toward a future circulation pattern conducive to extreme drying and heating in central North America during summer, particularly in association with greater instances of easterly flow aloft.

• This circulation change appears to be fostered by the enhanced summertime heating of continents in mid-high latitudes, which promotes an annular band of maximum height increases across the entire Northern Hemisphere. The amplified warmth over land and its remote influence are favored by diminishing snow cover and low terrestrial heat capacity in latitudes where land is especially prevalent.

Our analysis focuses on greater North America because its projected response to greenhouse forcing is considerably different from elsewhere in the Northern Hemisphere (Figure 6, Cattiaux et al. 2016, Peings et al. 2016). A distinguishing finding of this study is the latitudinally varying response of projected seasonal circulation changes, which reveal dipole changes in circulation vigor and waviness from north to south that are related to meridional shifts in jet stream location. This differentiation contrasts with the "block" approach taken by Barnes and Polvani (2015), who concluded that CMIP5 models generally simulate a weak Arctic influence on future circulation characteristics over the greater North American-Atlantic region, based on domain averages from 30°-70°N. Our study also refines recent findings by Cattiaux et al. (2016) and Peings et al. (2016), whose conclusions of future circulation changes in respective CMIP5 and LENS simulations were based on sinuosity centered at a fixed latitude (~50°N). Both of these studies identified a future increase (decrease) in sinuosity during winter (summer) over the North American sector, but our results demonstrate that this average response is the result of opposing changes in different zones within the domain.

One motivation for this work was to test the hypothesis of FV12 that Arctic amplification would lead to a weaker and wavier mid-latitude circulation that is more

524 conducive to prolonged extreme weather events. Our results provide partial support for
525 this hypothesis but reveal that the extratropical response is more geographically varied
526 than implied by that study. FV12's central physical mechanism is supported by our results,
527 in that simulated AA promotes ridging in mid-high latitudes that weakens the zonal wind
528 on the equatorward flank and leads to a wavier (more sinuous) flow. However, this
529 response is not uniform across the entire extratropical domain; instead, we find that some
530 areas exhibit the opposite pattern of troughing, stronger zonal winds, and reduced
531 waviness.

532 An open question is the extent to which the enhanced westerlies around 30°N during
533 winter (Figure 6e) originate from a tropically induced strengthening of the meridional
534 height gradient, as opposed to a direct mass-compensation response to AA itself (Figure 6c).
535 For example, during a negative AO phase the characteristic high-latitude ridging anomaly is
536 offset by a mid-latitude troughing anomaly (Thompson and Wallace 1998) associated with
537 stronger westerlies on its equatorward flank that resembles the atmospheric response to
538 tropical warming during El Niños. Because greenhouse forcing causes warming and height
539 inflation in upper levels of the tropical troposphere as well as in the lower polar
540 troposphere (Held 1993, Barnes and Screen 2015, Cattiaux et al 2016), isolating the Arctic
541 contribution to the strengthened westerlies during winter in the LENS simulations is
542 difficult. Further complicating this issue is the fact that Arctic warming is associated with
543 temperature increases elsewhere, thus leading indirectly to tropical heating anomalies.
544 However, some resolution of these competing influences is found in the CCSM4 model
545 experiments with prescribed future reductions in Arctic sea ice by Deser et al. (2015),
546 which showed that the induced Arctic warming from ice loss alone caused additional

547 warming in the upper-troposphere tropics along with significantly stronger westerlies
548 between 30^{o}-40^{o}N---even excluding SST changes elsewhere in the world---suggesting that
549 the additional tropical heating in their fully coupled simulation further strengthened the
550 zonal winds in this band.

551 Although our study does not provide a conclusive answer to the role of the Arctic in
552 affecting mid-latitude atmospheric circulation and weather extremes, it does augment the
553 body of evidence suggesting that AA exerts a remote climatic influence that is highly
554 variable by both latitude and season. In particular, our findings point to a potentially
555 important contribution from enhanced terrestrial Arctic warming during spring-summer, a
556 piece of the story that has been overshadowed by the widespread research focus on
557 wintertime heating from sea ice loss. However, the recent decline in hemispheric spring
558 snow-cover extent has actually outpaced the corresponding reduction in sea-ice coverage
559 in both absolute and relative terms (Derkson and Brown 2012). Assuming that spring
560 snow extent will continue its downward trend, the results from LENS suggest that this
561 change may have important repercussions beyond the Arctic by influencing the large-scale
562 extratropical circulation in a way that helps to explain the commonly simulated drying and
563 enhanced heating of interior North America.

564

565 **Acknowledgments**

566 This project has been supported by NSF grants PLR-1304398, PLR-1304097, AGS-1407360,
567 AGS-1203430, and AGS-1602771. Computing resources on the Yellowstone

568 supercomputer were provided by NCAR's Computational and Information Systems
569 Laboratory, sponsored by the National Science Foundation.

References

Alexander, M. A., R. Tomas, C. Deser, and D. M. Lawrence, 2010: The atmospheric response to projected terrestrial snow changes in the late 21st century. *J. Climate*, **23**, 6430-6437.

Barnes, E. A., 2013: Revisiting the evidence linking Arctic amplification to extreme weather in midlatitudes. *Geophys. Res. Lett.*, **40**, 4728–4733.

Barnes, E. A., E. Dunn-Sigouin, G. Masato, and T. Woolings, 2014: Exploring recent trends in Northern Hemisphere blocking. *Geophys. Res. Lett.*, **41**, 638–644.

Barnes, E. A., and L. M. Polvani, 2015: CMIP5 projections of Arctic amplification, of the North American/North Atlantic circulation, and of their relationship. *J. Climate*, **28**, 5254-5271**.**

Barnes, E. A. and J. A. Screen, 2015: The impact of Arctic warming on the midlatitude jet-stream: Can it? Has it? Will it? *WIREs Climate Change*, **6**, 277-286.

Barriopedro, D., R. Garcia-Herrera, A. R. Lupo, and E. Hernandez, 2006: A climatology of Northern Hemisphere blocking. *J. Climate*, **19**, 1042-1063.

Brewer, M. C., and C. F. Mass, 2016: Projected changes in western U. S. large-scale summer synoptic circulations and variability in CMIP5 models*. J. Climate*, **29**, 5965-5978.

Cattiaux, J., Y. Peings, D. Saint-Martin, N. Trou-Kechout, and S. J. Vavrus, 2016: Sinuosity of midlatitude atmospheric flow in a warming world*. Geophys. Res. Lett.,* **43**, 8259–8268.

Chang, E. K. M., Y. Guo, and X. Xia, 2012: CMIP5 multimodel ensemble projection of storm track change under global warming. *J. Geophys. Res.*, **117**, D23118, doi:10.1029/2012JD018578.

591 Chang, F.-C., and J. M. Wallace, 1987: Meteorological conditions during heat waves and
592 droughts in the United States Great Plains. *Mon. Wea. Rev*., **115**, 1253-1269.

593 Chen, G., J. Lu, D. A. Burrows, and L. R. Leung, 2015: Local finite-amplitude wave activity as
594 an objective diagnostic of midlatitude extreme weather. *Geophys. Res. Lett.,*
595 doi:10.1002/2015GL066959.

596 Cohen, J., J. Foster, M. Barlow, K. Saito, and J. Jones, 2010*:* Winter 2009–2010: A case study
597 of an extreme Arctic Oscillation event*. Geophys. Res. Lett.,* **37**, L17707*,*
598 doi:10.1029/2010GL044256*.*

599 Cohen, J., J. A. Screen, J. C. Furtado, M. Barlow, D. Whittleston, D. Coumou, J. Francis, K.
600 Dethloff, D. Entekhabi, J. Overland, J. Jones, 2014: Recent Arctic amplification and
601 extreme mid-latitude weather. *Nature Geosci.*, **7**, 627-637.

602 Coumou, D., J. Lehmann, J. Beckmann, 2015: The weakening summer circulation in the
603 Northern Hemisphere mid-latitudes. *Science*, **348**, 324-327.

604 Crawford, A., and M. Serreze, 2015: A new look at the summer Arctic frontal zone. *J. Climate*,
605 **28**, 737-754.

606 Dee, D. P., and 35 others, 2011: The ERA-Interim reanalysis: Configuration and
607 performance of the data assimilation system. *Q. J. R. Meteor. Soc*., **137**, 553–597.

608 Derksen, C., and R. Brown, 2012: Spring snow cover extent reductions in the 2008-2012
609 period exceeding climate model projections. *Geophys. Res. Lett.*, **39**, L19504,
610 doi:10.1029/2012GL053387.

611 Deser, C., R. A. Tomas, and L. Sun, 2015: The role of ocean-atmosphere coupling in the
612 zonal-mean atmospheric response to Arctic sea ice loss. *J. Climate*, **28**, 2168-2186.

613 Di Capua, G., and D. Coumou, 2016: Changes in meandering of the Northern Hemisphere
614 circulation. *Env. Res. Lett.*, doi:10.1088/1748-9326/11/9/094028.

615 Ding, Q., and B. Wang, 2005: Circumglobal teleconnection in the Northern Hemisphere
616 summer. *J. Climate*, **18**, 3483-3505.

617 Douville, H., J. Colin, E. Krug, J. Cattiaux, and S. Thao, 2016*:* Midlatitude daily summer
618 temperatures reshaped by soil moisture under climate change*. Geophys. Res. Lett.,* **43***,*
619 812–818.

620 Francis, J. A. and S. J. Vavrus, 2012: Evidence linking Arctic amplification to extreme
621 weather in mid-latitudes. *Geophys. Res. Lett.,* **39***,* doi:/10.1029/2012GL051000.

622 Francis, J., S. Vavrus, 2015: Evidence for a wavier jet stream in response to rapid Arctic
623 warming. *Environ. Res. Lett.*, **10**, 1, 014005.

624 Francis, J., and N. Skific, 2015: Evidence linking rapid Arctic warming to mid-latitude
625 weather patterns. *Phil. Trans. Roy. Soc. A*, doi:10.1098/rsta.2014.0170.

626 Gleason, K. L., J. H. Lawrimore, D. H. Levinson, T. R. Karl, and D. J. Karoly, 2008: A revised U.
627 S. Climate Extremes Index. *J. Climate*, **21**, 2124–2137.

628 Gregory, J. M., J. F. B. Mitchell, and A. J. Brady, 1997: Summer drought in northern
629 midlatitudes in a time-dependent CO_2 climate experiment. *J. Climate*, **10**, 662-686.

630 Held, I., 1993: Large-scale dynamics and global warming. *Bull. Am. Meteor. Soc.*, 74, 228-241.

631 Honda, M., J. Inoue, and S. Yamane, 2009: Influence of low Arctic sea-ice minima on
632 anomalously cold Eurasian winters. *Geophys. Res. Lett.*, **36**, L08707, doi:
633 10.1029/2008GL037079.

634 Huang, C. S., and N. Nakamura, 2016: Local finite-amplitude wave activity as a diagnostic of
635 anomalous weather events. *J. Atmos. Sci.,* **73**, 211-229.

636 Kalnay, E., and 21 others, 1996: The NCEP/NCAR 40-year reanalysis project, *Bull. Am.*
637 *Meteor. Soc*., **77**, 437-471.

638 Kay, J. E., and 20 others, 2015: The Community Earth System Model (CESM) Large
639 Ensemble Project: A community resource for studying climate change in the presence of
640 internal climate variability. *Bull. Amer. Meteor. Soc.*, **96**, 1333–1349.

641 Kennedy, D., T. Parker, T. Woolings, B. Harvey, and L. Shaffrey, 2016: The response of high-
642 impact blocking weather systems to climate change. *Geophys. Res. Lett*., 7250-7258.

643 Kentarchos, A. S., and T. D. Davies, 1998: A climatology of cutoff lows at 200 hPa in the
644 Northern Hemisphere, 1990–1994. *Int. J. Climatol*., **18**, 379–390.

645 Knutti, R., D. Masson, and A. Gettelman, 2013: Climate model genealogy: Generation CMIP5
646 and how we got there. *Geophys. Res. Lett.*, **40**, 1194-1199.

647 Kug, , J.-S., J.-H. Jeong, Y.-S. Jang, B-M. Kim, C. K. Folland, S.-K. Min, and S.-W. Son, 2015: Two
648 distinct influences of Arctic warming on cold winters over North America and East Asia.
649 *Nature Geosci.,* **8**, 759-762.

650 Lau, N.-C., and M. J. Nath, 2012: A model study of heat waves over North America:
651 Meteorological aspects and projections for the twenty-first century. *J. Climate*, **25**, 4761-
652 4784.

653 Lehmann, J., D. Coumou, K. Frieler, A. V. Eliseev, and A. Levermann, 2014: Future changes in
654 extratropical storm tracks and baroclinicity under climate change. *Env. Res. Lett.*, **9**,
655 084002.

656 Liu, J., J. A. Curry, H. Wang, M. Song, and R. M. Horton, 2012: Impact of declining Arctic sea
657 ice on winter snowfall, *PNAS*, **109**, 4074-4079.

658 Lu, J., G. A. Vecchi, and T. Reichler, 2007: Expansion of the Hadley cell under global warming.
659 *Geophys. Res. Lett.*, **34**, L06805, doi:10.1029/2006GL028443.

660 Madden, R. A., and J. Williams, 1978: The correlation between temperature and
661 precipitation in the United States and Europe. *Mon. Wea. Rev.*, **106**, 142-147.

662 Maloney, E. D., and 30 others, 2014: North American climate in CMIP5 experiments: Part
663 III: Assessment of twenty-first-century projections. *J. Climate*, **27**, 2230-2270.

664 Mann, H. B., 1945: Non-parametric tests against trend. *Econometrica*, **13**, 163-171.

665 Martin, J. E., S. J. Vavrus, F. Wang, and J. A. Francis, 2015: Sinuosity as a measure of middle
666 tropospheric waviness. J. Climate, in review.

667 Matsumura, S., and K. Yamazaki, 2012: Eurasian subarctic summer climate in response to
668 anomalous snow cover. *J. Climate*, **25**, 1305-1317.

669 Matsumura, S., X. Zhang, and K. Yamazaki, 2014: Summer Arctic atmospheric circulation
670 response to spring Eurasian snow cover and its possible linkage to accelerated sea ice
671 decrease. *J. Climate*, **27**, 6551-6558.

672 Meehl, G. A., and C. Tebaldi, 2004: More intense, more frequent, and longer lasting heat
673 waves in the 21st century. *Science*, **305**, 994-997.

674 Mo, K. C., J. N. Paegle, and R. W. Higgins, 1997: Atmospheric processes associated with
675 summer floods and droughts in the central United States. *J. Climate*, **10**, 3028-3046.

676 Nakamura, N., 1996: Two-dimensional mixing, edge formation, and permeability diagnosed
677 in an area coordinate. *J. Atmos. Sci.*, **53**, 1524-1537.

678 Nakamura, N., and A. Solomon, 2010: Finite-amplitude wave activity and mean flow
679 adjustments in the atmospheric general circulation. Part I: Quasigeostrophic theory and
680 analysis. *J. Atmos. Sci.*, **67**, 3967–3983.

681 Newson, R. L., 1973: Response of a general circulation model of the atmosphere to removal
682 of the Arctic ice cap. *Nature*, **241**, 39-40.

683 Otto-Bliesner, B. L., E. C. Brady, G. Clauzet, R. Tomas, S. Levis, and Z. Kothavala, 2006: Last
684 Glacial Maximum and Holocene climate in CCSM3. *J. Climate*, **19**, 2526-2544.

685 Overland, J. E., J. A. Francis, R. Hall, E. Hanna, S.-J. Kim, and T. Vihma, 2015: The melting
686 Arctic and midlatitude weather patterns: Are they connected? *J. Climate*, **28**, 7917-7932.

687 Peings, Y., J. Cattiaux, S. Vavrus, and G. Magnusdottir, 2016: Late 21st century changes of the
688 mid-latitude atmospheric circulation in the CESM Large Ensemble. *J. Climate*, in review.

689 Petoukhov, V., and V. Semenov, 2010: A link between reduced Barents-Kara sea ice and cold
690 winter extremes over northern continents. *J. Geophys. Res.,* **115***,* D21111,
691 doi:10.1029/2009JD013568*.*

692 Petoukhov, V., S. Rahmstorf, S. Petri, and H. J. Schellnhuber, 2013: Quasiresonant
693 amplification of planetary waves and recent Northern Hemisphere weather extremes.
694 *Proc. Natl. Acad. Sci*., **110**, 5336-5341.

695 Price, J. D., and G. Vaughan, 1992: Statistical studies of cutoff-low systems. *Ann. Geophys*., **10**,
696 96–102.

697 Rivière, G., 2011: A dynamical interpretation of the poleward shift of the jet streams in
698 global warming scenarios. *J. Atmos. Sci.,* **68**, 1253–1272.

699 Rohli, R. V., K. M. Wrona, and M. J. McHugh, 2005: January northern hemisphere
700 circumpolar vortex variability and its relationship with hemispheric temperature and
701 regional teleconnections. *Int. J. Climatol*., **25**, 1421-1436.

702 Rossby, C.-G., and collaborators, 1939: Relations between variations in the intensity of the
703 zonal circulation of the atmosphere and the displacements of the semi-permanent
704 centers of action. *J. Marine Res*., **2**, 38-54.

705 Rowell, D. P., and R. G. Jones, 2006: Causes and uncertainty of future summer drying over
706 Europe. *Climate Dyn*., **27**, 281-299.

707 Rowell, D. P., 2009: Projected midlatitude continental summer drying: North America
708 versus Europe*. J. Climate*, **22**, 2813-2833.

709 Scheff, J., and D. M. W. Frierson, 2012: Robust future precipitation declines in CMIP5 largely
710 reflect the poleward expansion of model subtropical dry zones. *Geophys. Res. Lett.*, **39**,
711 L18704, doi:10.1029/2012GL052910.

712 Screen, J. A., and I. Simmonds, 2013: Exploring links between Arctic amplification and mid-
713 latitude weather. *Geophys. Res. Lett.*, **40**, 959-964.

714 Screen, J. A., and I. Simmonds, 2014: Amplified mid-latitude planetary waves favour
715 particular regional weather extremes. *Nat. Climate Change*, **4**, 704–709.

716 Sen, P. K., 1968: Estimates of the regression coefficient based on Kendall's tau. *J. Am. Stat.*
717 *Assoc.*, **63**, 1379-1389.

718 Singh, D. S., D. L. Swain, J. S. Mankin, D. E. Horton, L. N. Thomas, B. Rajaratnam and N. S.
719 Diffenbaugh, 2016: Recent amplification of the North American winter temperature
720 dipole. *Journal of Geophysical Research*, **121**, doi:10.1002/2016JD025116.

721 Su, H., Z.-L. Yang, R. E. Dickinson, and J. Wei, 2014: Spring soil moisture-precipitation
722 feedback in the Southern Great Plains: How is it related to large-scale atmospheric
723 conditions? *Geophys. Res. Lett.*, **41**, 1283-1289.

724 Teng, H., G. W. Branstator, G. A. Meehl, and W. M. Washington, 2016: Projected intensification
725 of subseasonal temperature variability and heat waves in the Great Plains. *Geophys. Res.*
726 *Lett.*, **43**, 2165-2173.

727 Thompson, D. W. J., and J. M. Wallace, 1998: The Arctic Oscillation signature in the
728 wintertime geopotential height and temperature fields. *Geophys. Res. Lett.*, **25**, 1297-
729 1300.

730 Thompson, D. W. J., and J. M. Wallace, 2001: Regional climate impacts of the northern
731 hemisphere annular mode. *Science*, **293**, 85-88.

732 Trenberth, K. E., and D. J. Shea, 2005: Relationships between precipitation and surface
733 temperature. *Geophys. Res. Lett.*, **32**, L14703, doi:10.1029/2005GL022760.

734 Vavrus, S., 2007: The role of terrestrial snow cover in the climate system. *Clim. Dyn*., **29**, 73-
735 88.

736 Vihma, T., 2014: Effects of Arctic sea ice decline on weather and climate: A review. *Surv.*
737 *Geophys*., **35**, 1175–1214.

738 Walsh, J. E., 2014: Intensified warming of the Arctic: Causes and impacts on middle
739 latitudes. *Glob. Planet. Change*, **117**, 52-63.

740 Wang, L., and N. Nakamura, 2015: Covariation of finite-amplitude wave activity and the
741 zonal mean flow in the midlatitude troposphere: 1. Theory and application to the
742 Southern Hemisphere summer*. Geophys. Res. Lett.,* **42***,* 8192–8200.

743 Warshaw, M., and R. R. Rapp, 1973: An experiment on the sensitivity of a global circulation
744 model. *J. Appl. Meteor*., **3**, 43-49.

745 Wetherald, R. T., and S. Manabe, 1999: Detectability of summer dryness caused by
746 greenhouse warming. *Climatic Change*, **43**, 495-511.

747 Willson, M. A. G., 1975: A wavenumber-frequency analysis of large-scale tropospheric
748 motions in the extratropical Northern Hemisphere. *J. Atmos. Sci*., **32**, 478-488.

749 Wrona, K. M., and R. V. Rohli, 2007: Seasonality of the northern hemisphere circumpolar
750 vortex. *Int. J. Climatol*., **27**, 697-713.

751 Yang, J., Q. Liu, Z. Liu, L. Wu, and F. Huang, 2009: Basin mode of Indian Ocean sea surface
752 temperature and Northern Hemisphere teleconnection. *Geophys. Res. Lett*., **36**, L19705,
753 doi:10.1029/2009GL039559.

754

Figure Captions

Figure 1. Example of sinuosity calculations for simple hemispheric and complex regional cases. (left) Blue line is a geopotential height contour at 500 hPa. The area enclosed poleward of that contour is equal to the area within the red circle, the equivalent latitude. Sinuosity equals the ratio of the length of the blue curve to the length of the red circle. (right) Example of regional sinuosity in a flow with multiple features. Using the most complex case of the 5280 m isohypse as an example, sinuosity is based on the combined length of all isohypse segments bounding the shading. This sum is divided by the arc length of the equivalent latitude determined by the sum of all shaded areas. See text for additional explanation.

Figure 2. Examples of noteworthy circulation states, illustrated by 500 hPa geopotential heights in dm. (a) Lowest ASIN on record (1.04, (b) Highest ASIN (2.64), (c) Extreme cold-air outbreak in January 2014 (ASIN = 95th percentile for January), and (d) Superstorm Sandy (ASIN = 98th percentile for October).

Figure 3. Annual cycle of sinuosity and zonal wind speed (m s^{-1}) at 500 hPa. Aggregate SIN from 1948-2014 in red and zonal wind speed in green from (a) reanalysis and (c) LENS. The zonal wind curve was calculated in the same weighted manner as aggregate SIN, based on the zonally averaged westerly wind speed across each isohypse. Zonally averaged sinuosity at individual isohypses comprising aggregate SIN from (b) reanalysis and (d)

776 LENS. Individual ensemble members are shown in light shading, and ensemble means are
777 represented in bold.

778

779 Figure 4. Mean annual aggregate SIN and linear trend line from 1948-2014 using reanalysis
780 data.

781

782 Figure 5. Moving linear trends of (left) sinuosity (per decade) and (right) 500 hPa zonal
783 wind speed (m s^{-1} yr^{-1}) from reanalysis during (top) DJF and (bottom) JJA. The trends
784 begin in a given year on the x axis and end in 2014. Stippling denotes significant trends at
785 the 90% confidence level using a least-squares regression.

786

787 Figure 6. Future changes (2081-2100 vs. 1981-2000) in (a, b): 2-m air temperature (K), (c,
788 d) 500 hPa heights (m), and (e, f) 500 hPa zonal wind speed (m s^{-1}) during (left) January
789 and (right) August. Shaded regions denote where the ensemble-mean changes are larger
790 than the standard deviation of the intra-ensemble changes. Dashed contours indicate
791 where wind speed changes are negative.

792

793 Figure 7: As in Figure 6 but for changes in (blue) zonal wind speed (m s^{-1}, upper x axis) and
794 (red) sinuosity (unitless, bottom x axis) during (top) January and (bottom) August over the
795 greater North American domain. Thin lines denote individual ensemble members, and
796 bold lines are the ensemble average. Solid bold lines indicate where the ensemble-mean
797 change exceeds the standard deviation of changes among all ensemble members.

798

799 Figure 8: Future changes (2081-2100 vs. 1981-2000) in August precipitation expressed as
800 (top) absolute difference (mm day^{-1}) and (bottom) percentage difference. The box over the
801 Plains denotes the reference region of especially pronounced drying and heating.

802

803 Figure 9: Daily mean 2-m air temperatures and rainfall over the mid-continental box (see
804 Fig. 8) for all August days as a function of the 500 hPa zonal wind speed (percentile) during
805 the (a, c) late 20th century and (b, d) late 21st century. High percentiles indicate a strong
806 westerly wind aloft, and low percentiles represent either a weak westerly wind or an
807 easterly wind. (e) Histogram of daily August wind speeds (m s^{-1}) in the late 20^{th} and late
808 21^{st} century. (f) Percentage change in August wind speed frequency during the late 21^{st}
809 century relative to the late 20^{th} century.

810

811 Figure 10: 500 hPa geopotential height (m) and wind velocity (m s^{-1}) anomalies in LENS on
812 the driest 5% of August months during the (left) late 20th century and (right) late 21st
813 century, relative to each time period's climatology. The box corresponds to the region of
814 enhanced drying and heating shown in Figure 8.

815

816 Figure 11: Future changes (2081-2100 vs. 1981-2000) in (a) MAM and (b) JJA snow
817 fraction averaged among all ensemble members in LENS.

818

819 Figure 12: Simulated changes in 2-m air temperature and 500 hPa geopotential heights
820 during June-August in two climate model simulations that produced amplified high-latitude
821 warming. (left) CCSM3 climate model driven by contemporary greenhouse forcing (year
822 1990) but with all terrestrial snow cover eliminated [from Vavrus 2007]. (right) CCSM4
823 paleoclimate simulation of 6,000 years ago minus year 1850 driven by differences in
824 Earth's orbital configuration between the two time periods.

Click here to download Rendered Figure
Figure1_revised.pdf

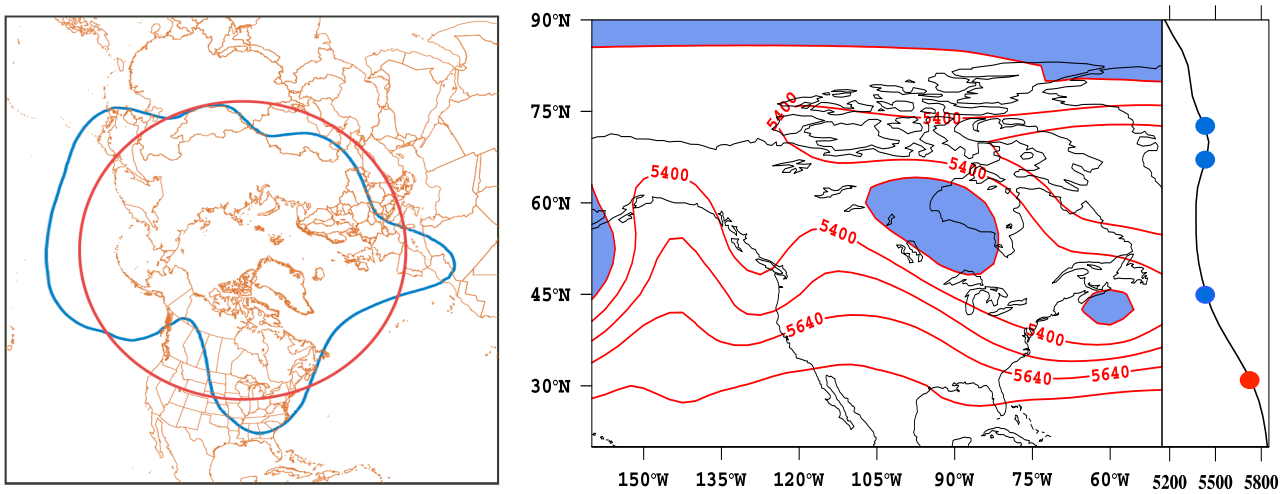

Figure 1. Example of sinuosity calculations for simple hemispheric and complex regional cases. (left) Blue line is a geopotential height contour at 500 hPa. The area enclosed poleward of that contour is equal to the area within the red circle, the equivalent latitude. Sinuosity equals the ratio of the length of the blue curve to the length of the red circle. (right) Example of regional sinuosity in a flow with multiple features. Using the most complex case of the 5280 m isohypse as an example, sinuosity is based on the combined length of all isohypse segments bounding the shading. This sum is divided by the arc length of the equivalent latitude determined by the sum of all shaded areas. See text for additional explanation.

Click here to download Rendered Figure
Figure2_revised.pdf

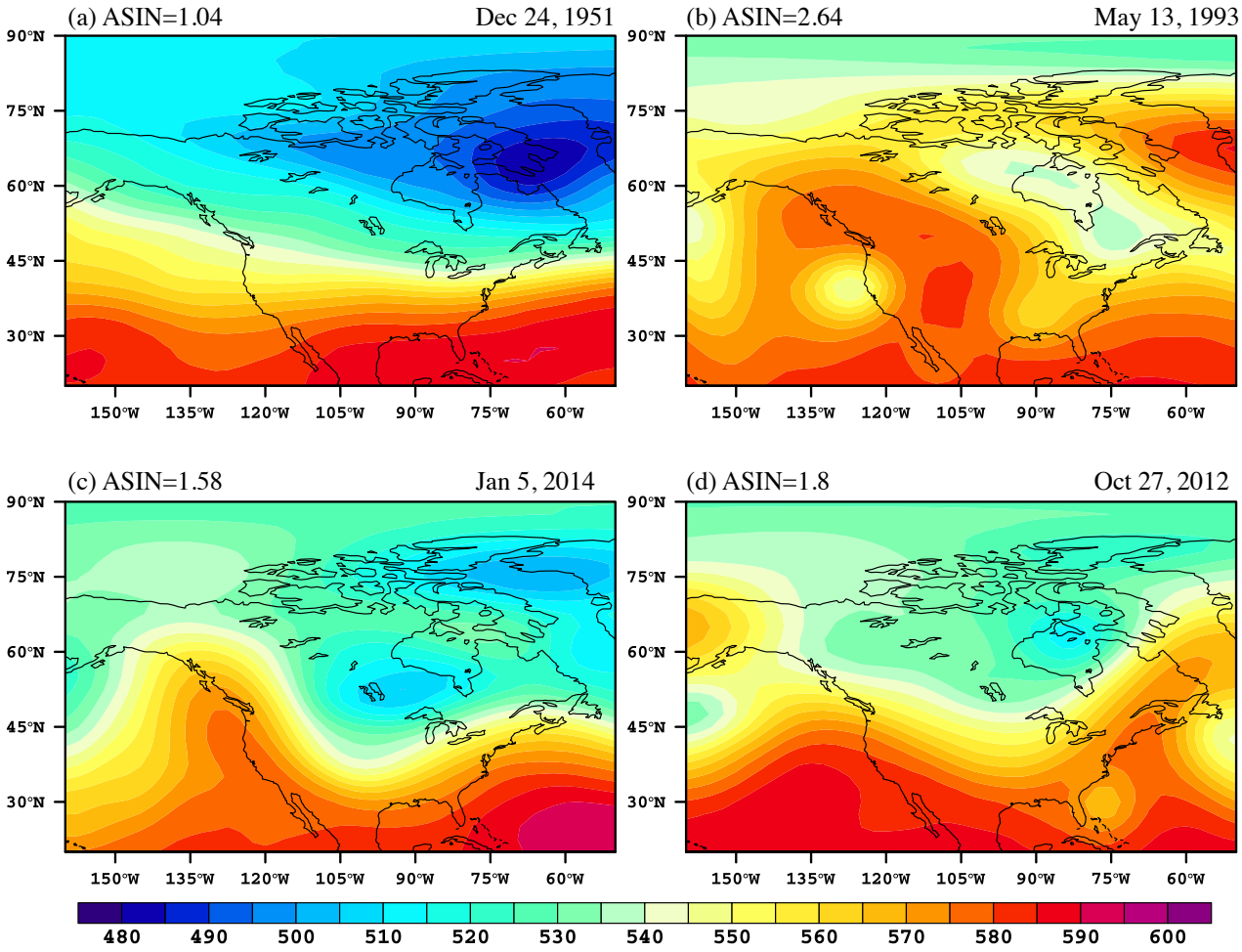

Figure 2. Examples of noteworthy circulation states, illustrated by 500 hPa geopotential heights in dm. (a) Lowest ASIN on record (1.04), (b) Highest ASIN (2.64), (c) Extreme cold-air outbreak in January 2014 (ASIN = 95th percentile for January), and (d) Superstorm Sandy (ASIN = 98th percentile for October).

Click here to download Rendered Figure
Figure3_revised.pdf

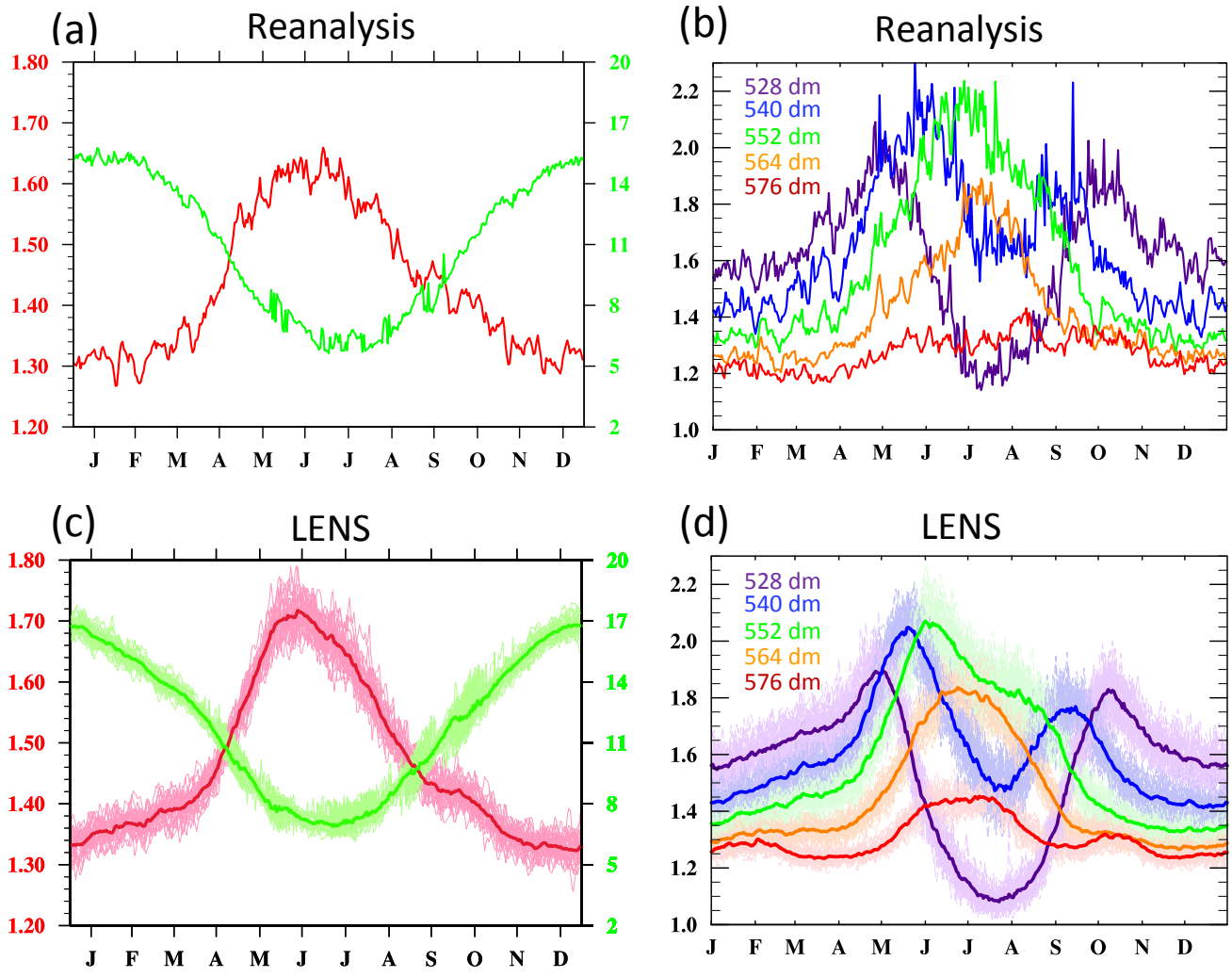

Figure 3. Annual cycle of sinuosity and zonal wind speed (m s^{-1}) at 500 hPa. Aggregate SIN from 1948-2014 in red and zonal wind speed in green from (a) reanalysis and (c) LENS. The zonal wind curve was calculated in the same weighted manner as aggregate SIN, based on the zonally averaged westerly wind speed across each isohypse. Zonally averaged sinuosity at individual isohypses comprising aggregate SIN are shown from (b) reanalysis and (d) LENS. Individual ensemble members are shown in light shading, and ensemble means are represented in bold.

Click here to download Rendered Figure
Figure4_revised.pdf

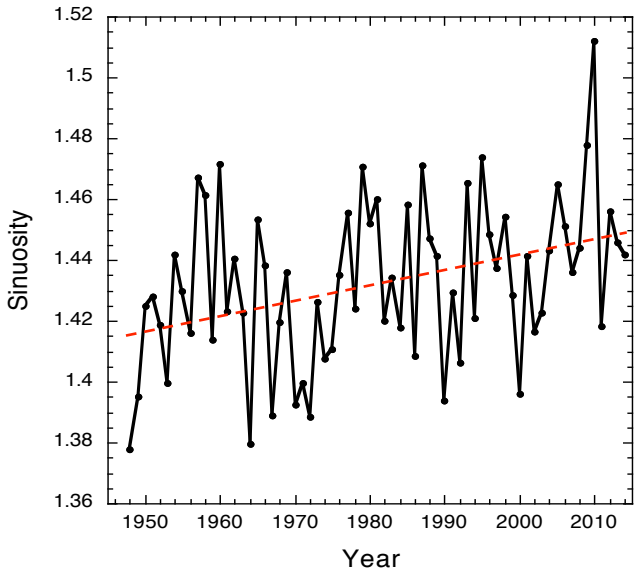

Figure 4. Mean annual aggregate SIN and linear trend line from 1948-2014 using reanalysis data.

Click here to download Rendered Figure
Figure5_revised.pdf

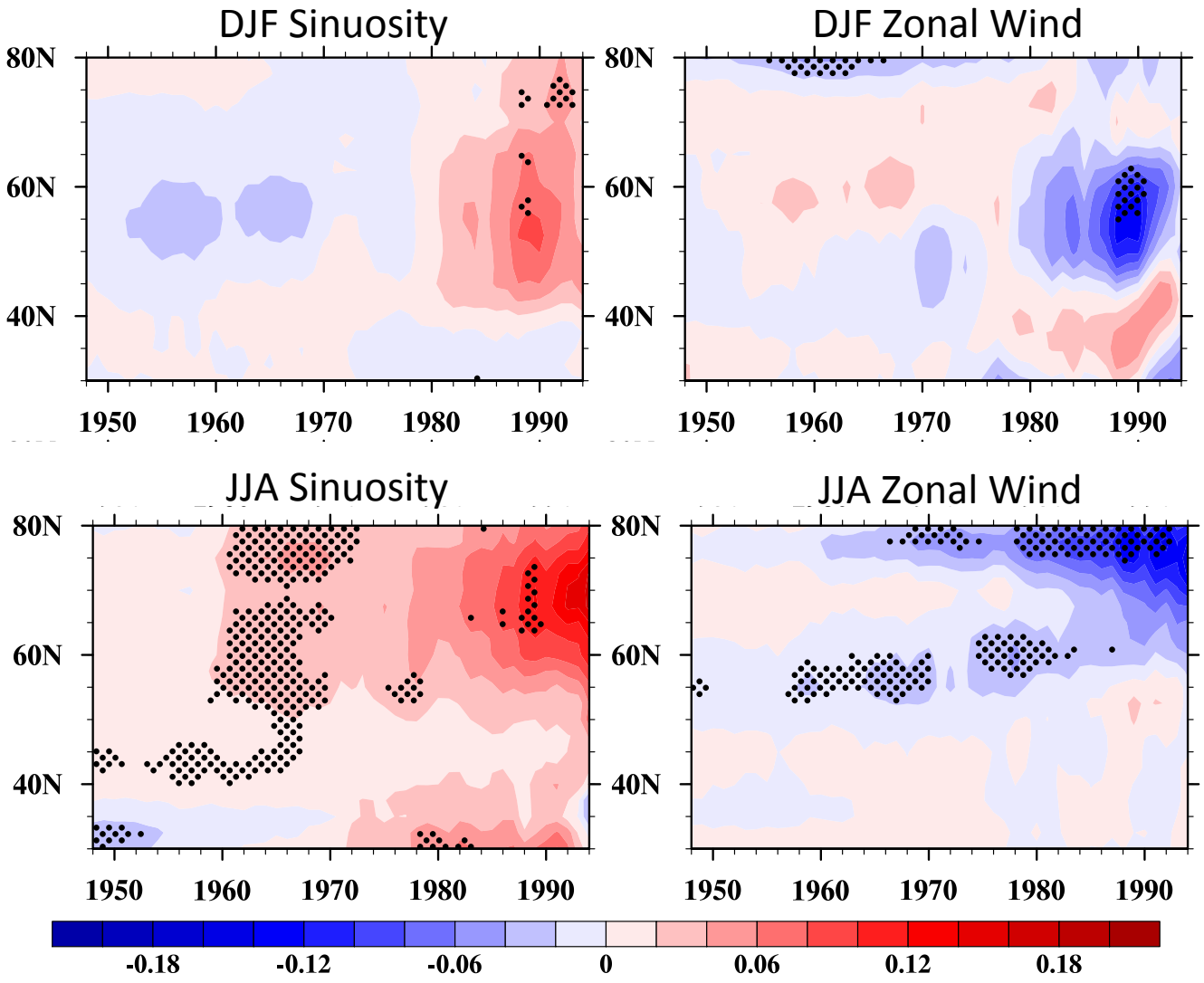

Figure 5. Moving linear trends of (left) sinuosity (per decade) and (right) 500 hPa zonal wind speed (m s^{-1} yr^{-1}) from reanalysis during (top) DJF and (bottom) JJA. The trends begin in a given year on the x axis and end in 2014. Stippling denotes significant trends at the 90% confidence level using a least-squares regression.

Figure 6

Click here to download Rendered Figure
Figure6_revised.pdf

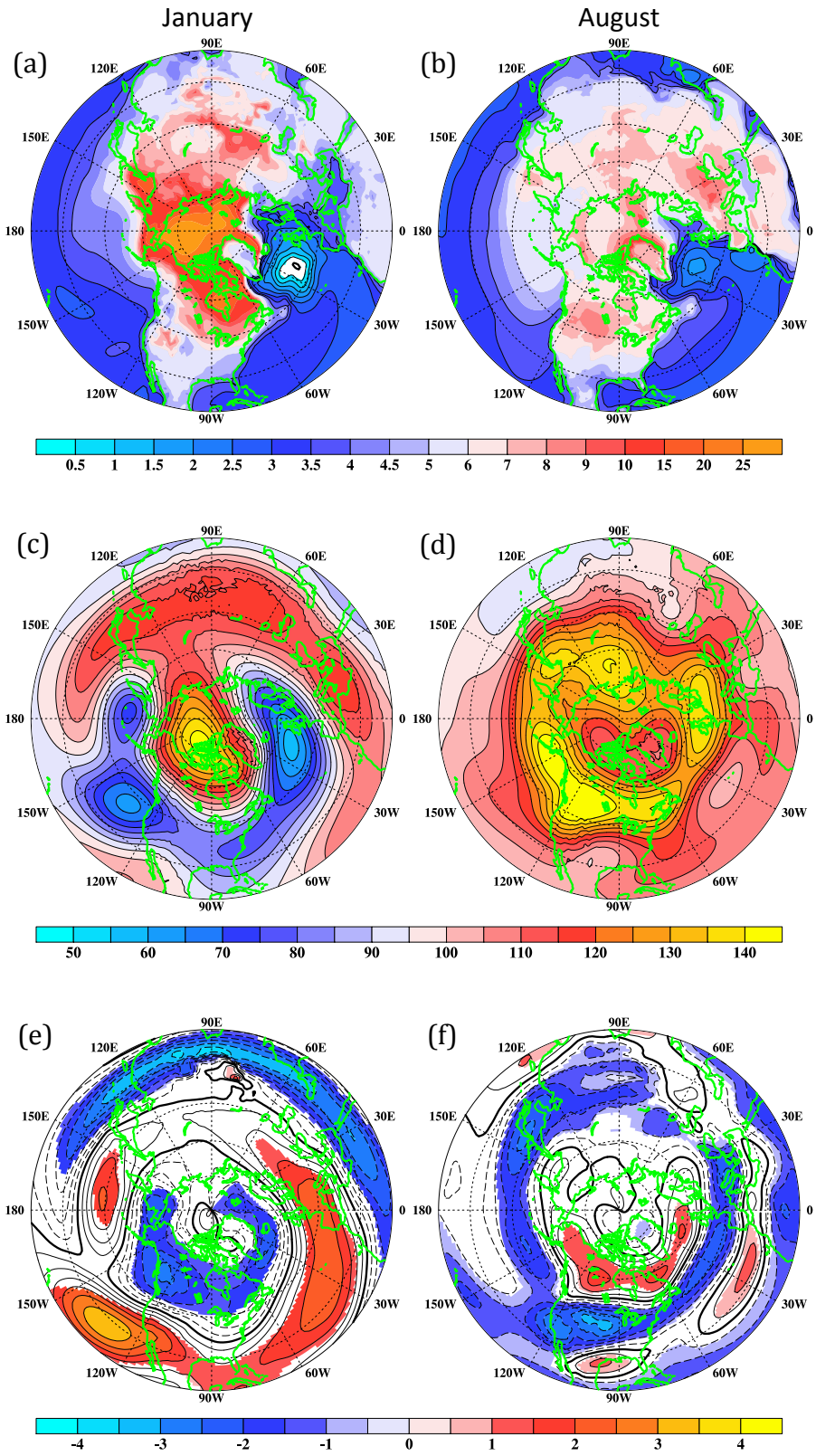

Figure 6. Future changes (2081-2100 vs. 1981-2000) in (a, b): 2-m air temperature (K), (c, d) 500 hPa heights (m), and (e, f) 500 hPa zonal wind speed (m s^{-1}) during (left) January and (right) August. Shaded regions denote where the ensemble-mean changes are larger than the standard deviation of the intra-ensemble changes. Dashed contours indicate where wind speed changes are negative.

Figure 7

Click here to download Rendered Figure
Figure7_revised.pdf

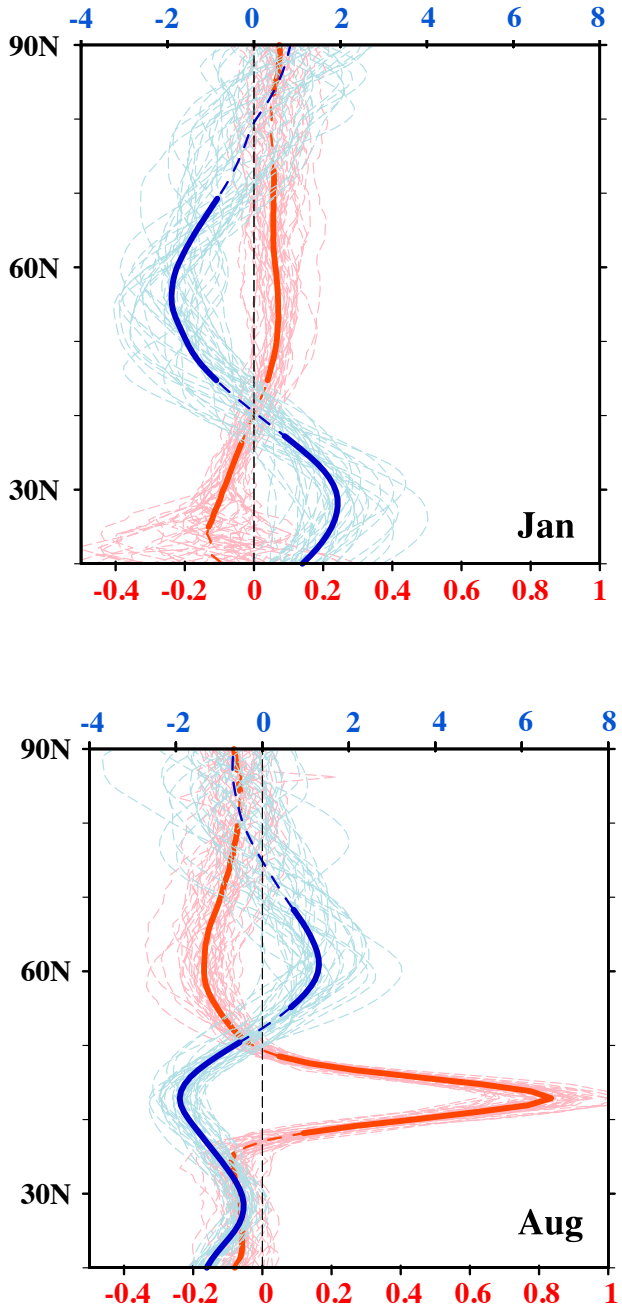

Figure 7: As in Figure 6 but for changes in (blue) zonal wind speed (m s^{-1}, upper x axis) and (red) sinuosity (unitless, bottom x axis) during (top) January and (bottom) August over the greater North American domain. Thin lines denote individual ensemble members, and bold lines are the ensemble average. Solid bold lines indicate where the ensemble-mean change exceeds the standard deviation of changes among all ensemble members.

Click here to download Rendered Figure
Figure8_revised.pdf

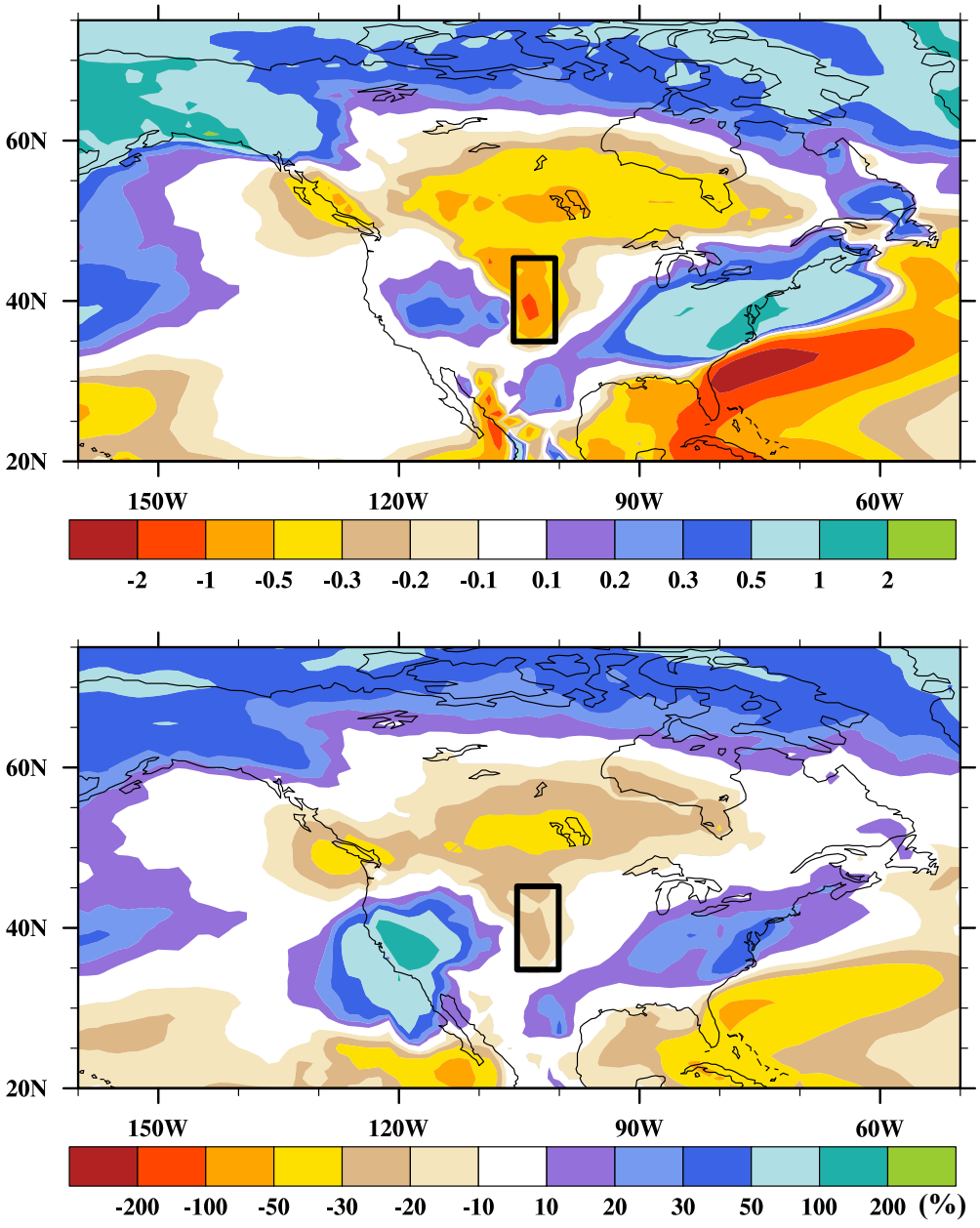

Figure 8: Future changes (2081-2100 vs. 1981-2000) in August precipitation expressed as (top) absolute difference (mm day^{-1}) and (bottom) percentage difference. The box over the Plains denotes the reference region of especially pronounced drying and heating.

Click here to download Rendered Figure
Figure9_revised.pdf

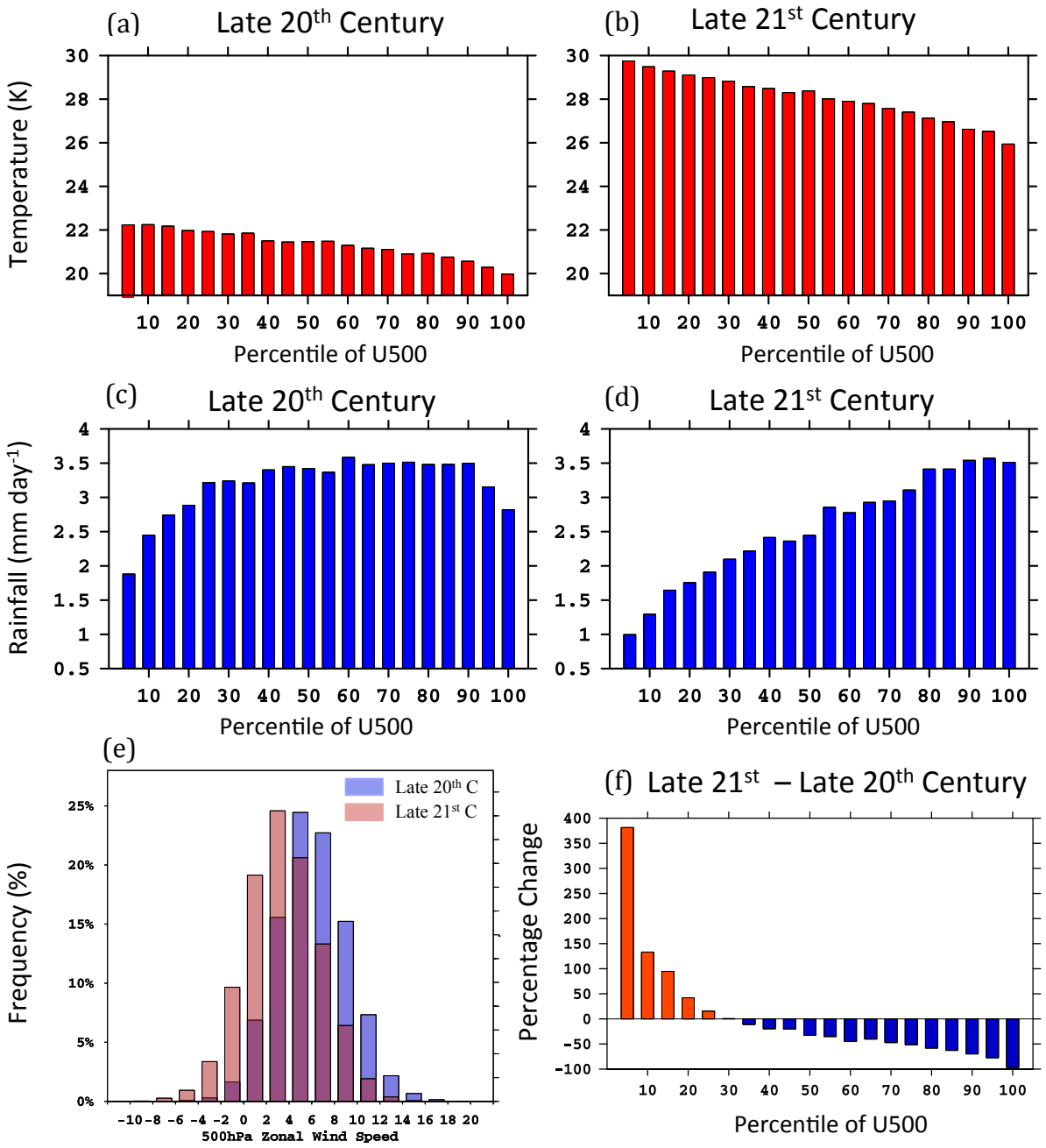

Figure 9: Daily mean 2-m air temperatures and rainfall over the mid-continental box (see Fig. 8) for all August days as a function of the 500 hPa zonal wind speed (percentile) during the (a, c) late 20th century and (b, d) late 21st century. High percentiles indicate a strong westerly wind aloft, and low percentiles represent either a weak westerly wind or an easterly wind. (e) Histogram of daily August wind speeds (m s^{-1}) in the late 20th and late 21st century. (f) Percentage change in August wind speed frequency during the late 21st century relative to the late 20th century.

Click here to download Rendered Figure
Figure10_revised.pdf

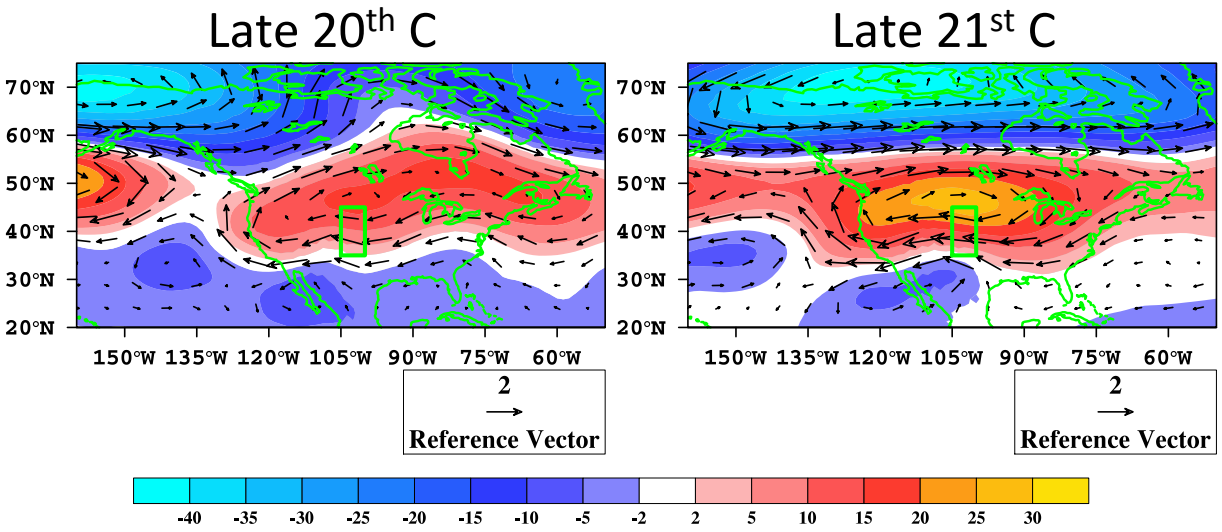

Figure 10: 500 hPa geopotential height (m) and wind velocity (m s^{-1}) anomalies in LENS on the driest 5% of August months during the (left) late 20th century and (right) late 21st century, relative to each time period's climatology. The box corresponds to the region of enhanced drying and heating shown in Figure 8.

Click here to download Rendered Figure
Figure11_revised.pdf

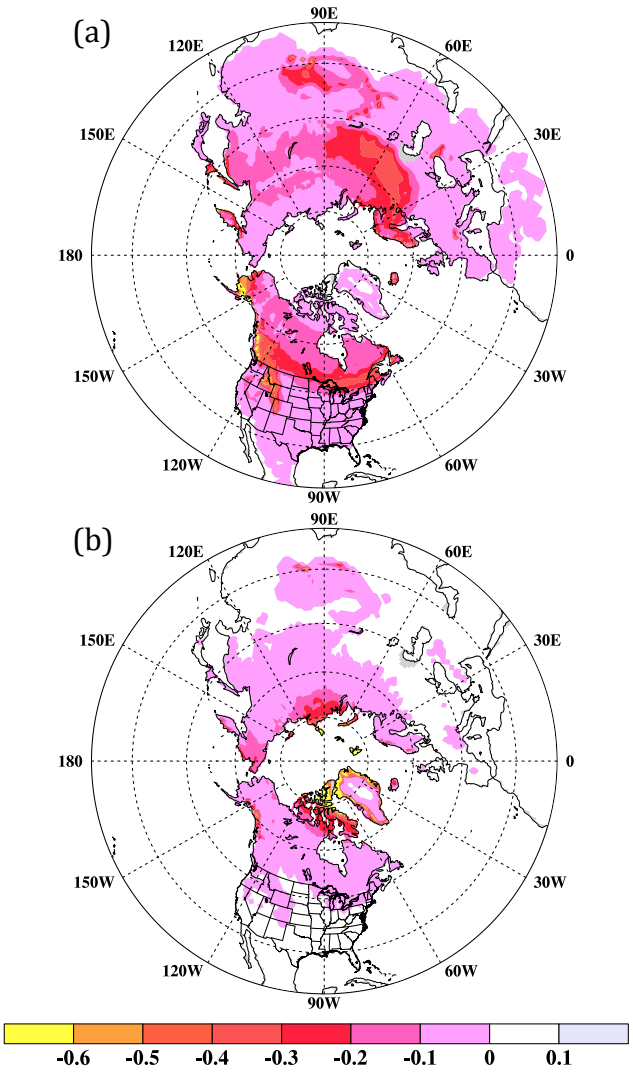

Figure 11: Future changes (2081-2100 vs. 1981-2000) in (a) MAM and (b) JJA snow fraction averaged among all ensemble members in LENS.

Click here to download Rendered Figure
Figure12_revised.pdf

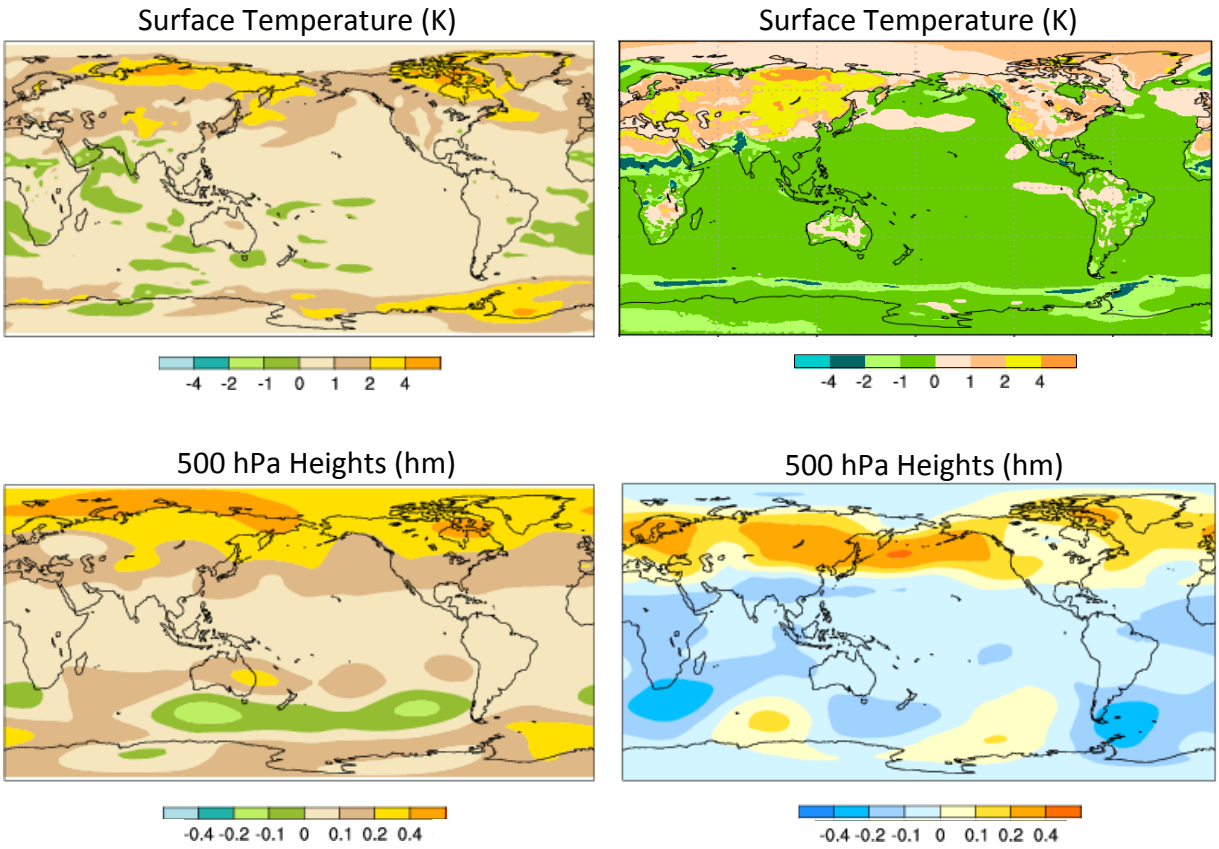

Figure 12: Simulated changes in 2-m air temperature and 500 hPa geopotential heights during June-August in two climate model simulations that produced amplified high-latitude warming. (left) CCSM3 climate model driven by contemporary greenhouse forcing (year 1990) but with all terrestrial snow cover eliminated [from Vavrus 2007]. (right) CCSM4 paleoclimate simulation of 6,000 years ago minus year 1850 driven by differences in Earth's orbital configuration between the two time periods.

Click here to access/download
Supplemental Material
Supplemental_Figures_revised.pdf